

Transportation Science

Publication details, including instructions for authors and subscription information:
<http://pubsonline.informs.org>

Lighthill-Whitham-Richards Model for Traffic Flow Mixed with Cooperative Adaptive Cruise Control Vehicles

Yanyan Qin , Hao Wang *, Daiheng Ni

To cite this article:

Yanyan Qin , Hao Wang *, Daiheng Ni (2021) Lighthill-Whitham-Richards Model for Traffic Flow Mixed with Cooperative Adaptive Cruise Control Vehicles. *Transportation Science* 55(4):883-907. <https://doi.org/10.1287/trsc.2021.1057>

Full terms and conditions of use: <https://pubsonline.informs.org/Publications/Librarians-Portal/PubsOnLine-Terms-and-Conditions>

This article may be used only for the purposes of research, teaching, and/or private study. Commercial use or systematic downloading (by robots or other automatic processes) is prohibited without explicit Publisher approval, unless otherwise noted. For more information, contact permissions@informs.org.

The Publisher does not warrant or guarantee the article's accuracy, completeness, merchantability, fitness for a particular purpose, or non-infringement. Descriptions of, or references to, products or publications, or inclusion of an advertisement in this article, neither constitutes nor implies a guarantee, endorsement, or support of claims made of that product, publication, or service.

Copyright © 2021, INFORMS

Please scroll down for article—it is on subsequent pages



With 12,500 members from nearly 90 countries, INFORMS is the largest international association of operations research (O.R.) and analytics professionals and students. INFORMS provides unique networking and learning opportunities for individual professionals, and organizations of all types and sizes, to better understand and use O.R. and analytics tools and methods to transform strategic visions and achieve better outcomes.

For more information on INFORMS, its publications, membership, or meetings visit <http://www.informs.org>

Lighthill-Whitham-Richards Model for Traffic Flow Mixed with Cooperative Adaptive Cruise Control Vehicles

Yanyan Qin,^{a,b} Hao Wang,^{b,*} Daiheng Ni^c

^aSchool of Traffic and Transportation, Chongqing Jiaotong University, Chongqing 400074, China; ^bSchool of Transportation, Jiangsu Key Laboratory of Urban ITS, Jiangsu Province Collaborative Innovation Center of Modern Urban Traffic Technologies, Southeast University, Nanjing 210096, China; ^cDepartment of Civil and Environmental Engineering, University of Massachusetts, Amherst, Massachusetts 01003

*Corresponding author

Contact: qinyanyan@cqjtu.edu.cn,  <https://orcid.org/0000-0002-1810-9202> (YQ); haowang@seu.edu.cn,  <https://orcid.org/0000-0001-7961-7588> (HW); ni@ecs.umass.edu,  <https://orcid.org/0000-0002-7401-8700> (DN)

Received: June 15, 2017

Revised: February 5, 2018; April 29, 2019;
August 13, 2020

Accepted: March 5, 2021

Published Online in Articles in Advance:
June 29, 2021

<https://doi.org/10.1287/trsc.2021.1057>

Copyright: © 2021 INFORMS

Abstract. In the future, road traffic will incorporate a random mix of manual vehicles and cooperative adaptive cruise control (CACC) vehicles, where a CACC vehicle will degrade to an adaptive cruise control (ACC) vehicle when vehicle-to-vehicle communications are not available. This paper proposes a generalized framework of the Lighthill-Whitham-Richards (LWR) model for such mixed vehicular flow under different CACC penetration rates. In this approach, the kinematic wave speed propagating through the mixed platoon was theoretically proven to be the slope of mixed fundamental diagram. In addition, the random degradation from CACC to ACC was captured in mathematical expectation for traffic scenarios where the CACC only monitors one vehicle ahead. Three concrete car-following models, the intelligent driver model (IDM) and CACC/ACC models validated by Partners for Advanced Transit and Highways (PATH) program, were selected as examples to investigate the propagation of small perturbations and shock waves. Numerical simulations were also performed based on the selected car-following models. Moreover, the derived mixed LWR model was applied to solve some traffic flow problems. It indicates that the proposed LWR model is able to describe the propagation properties of both small perturbations and shock waves. The mixed LWR model can also be used to solve some practical problems, such as the queue caused by a traffic accident and the impact of a moving bottleneck. More importantly, the proposed generalized framework admits other CACC/ACC/regular car-following models, including those developed from further experiments.

Funding: This work was supported by the National Natural Science Foundation of China [Grants 52002044, 51878161, and 52072067].

Keywords: cooperative adaptive cruise control (CACC) • mixed traffic flow • LWR model • simulations • car-following model • connected and automated vehicles

1. Introduction

In the last few decades, connected vehicle and intelligent vehicle technology such as adaptive cruise control (ACC) and cooperative adaptive cruise control (CACC) have been developed to improve safety and dynamics of traffic flow (Shladover et al. 2015). ACC systems adjust vehicle speed and maintain a desired distance to the preceding vehicle based on a preselected time gap (Weinberger, Winner, and Bubb 2001). In the early stage, the dynamics of ACC were extensively studied based on microscopic traffic flow models, such as car-following models (Davis 2004, Kesting et al. 2008, Kesting, Treiber, and Helbing 2010). Additionally, Monte Carlo simulations (Jerath et al. 2015) and the three-phase traffic theory (Kerner 2016) were also used to study the performance of traffic flow mixed with ACC vehicles. However, most analytical and simulation-based analyses of ACC performance

in existing literature have not been validated using experimental data. Fortunately, the experimental tests were carried out with production vehicles equipped with a commercial ACC system (Milanés and Shladover 2014). Although the commercially available ACC control system is designed with serious consideration of stability, and is actually more stable than some other factory systems, experimental results indicate that it is still unstable when applied to real vehicles at the present stage (Milanés and Shladover 2014, Wang et al. 2019).

CACC is a further development of ACC that adds vehicle-to-vehicle (V2V) communications. Microscopic models were used to show that CACC vehicles can improve the stability and capacity of traffic flow (Van Arem, Van Driel, and Visser 2006, Zhou and Ahn 2019). The macroscopic model for CACC traffic flow dynamics was also developed from the gas-kinetic theory (Ngoduy 2013a, Delis, Nikolos, and Papageorgiou

2015). It was found that CACC enhances the stability of traffic flow with respect to both small and large perturbations. Additionally, some CACC controller implementations in production vehicles were performed (Ge et al. 2018, Ploeg et al. 2011, van Nunen et al. 2012); these tests indicated that CACC benefits the stability of traffic flow and provide valuable experience for bringing the CACC control technology into production (Milanés et al. 2014). However, these control technologies (Geiger et al. 2012, Guvenc et al. 2012) cannot easily be directly transformed into CACC car-following models. To deal with this problem, a car-following model was developed based on a CACC control system implemented in real vehicles (Milanés and Shladover 2014, Milanés et al. 2014). Based on the experimental data, this CACC car-following model was validated to match the car-following performance of real CACC vehicles quite well. Importantly, the results show that CACC vehicles can smooth the perturbation waves and then enhance the stability of traffic flow.

Based on the previous statement, it is believed that CACC should be developed preferentially as one of the intelligent vehicle technologies. Because the market penetration level of CACC vehicles will gradually increase over a long period of times, future traffic flow will contain a random mix of manual vehicles and CACC vehicles. Manual vehicles will often appear in mixed traffic scenarios in the early stages of CACC market penetration. A CACC vehicle cannot obtain driving data from preceding vehicles when the preceding vehicles are manual vehicles without V2V communication devices. In that case, CACC inherently degrades to ACC, which serves as an alternative fallback scenario (Ploeg et al. 2015, Wang et al. 2019). Therefore, the ACC system is still needed when this degradation case happens.

Although this mixed traffic flow is likely to be realistic in the near future, its characteristics are not fully discussed (Mahmassani 2016, Talebpour and Mahmassani 2016, Gong, Zhou, and Peeta 2019, Chen et al. 2020, Zhong et al. 2020, Zhou and Zhu 2021). Much research has been conducted for microscopic car-following models of CACC/ACC traffic flow (Gong, Shen, and Du 2016; Jia and Ngoduy 2016a, b; Navas and Milanés 2019; Xiao et al. 2019; Ngoduy and Li 2021; Wang et al. 2020; Zhou and Zhu 2020). Comparatively speaking, its macroscopic continuum models are relatively less studied (Ngoduy 2013b, Jin 2016). The macroscopic continuum models are of great importance to the dynamic analysis of large-scale traffic flow mixed with CACC and ACC vehicles. In particular, the Lighthill-Whitham-Richards (LWR) model (Lighthill and Whitham 1955, Richards 1956) has been central in many studies on traffic dynamics because of its simplicity and strong ability to capture kinematic shock and rarefaction waves in traffic flow. The LWR model has been extended to mixed vehicular flow to analyze some puzzling traffic phenomena. The multiclass LWR model (Treiber

and Helbing 1999, Hoogendoorn and Bovy 2000, Wong and Wong 2002, Benzoni-Gavage and Colombo 2003, Ngoduy and Liu 2007, Loggne and Immers 2008, Van Lint, Hoogendoorn, and Schreuder 2008, Ngoduy 2010, van Wageningen-Kessels et al. 2014, Qian et al. 2017) and the multicommodity LWR model (Daganzo 1997, 2002; Daganzo, Lin, and Del Castillo 1997; Zhang and Jin 2002; Jin 2013; Jin, Gan, and Lebacque 2015; Shiomi et al. 2015) were developed to study dynamics of heterogeneous drivers, lane-changing traffic flow, and traffic networks. They reveal that the fundamental diagram is indispensable in almost all extended LWR models. It is noteworthy that, in some efforts, the LWR model was investigated with the probabilistic fundamental diagram (Ngoduy 2011, Li et al. 2012, Tang et al. 2012). Such LWR modeling describes the random variation of driving behavior. To our best knowledge, however, no published record was found that has presented extensions of the LWR model based on mixed fundamental diagram with different CACC penetration rates. Therefore, this article studies the LWR model of mixed traffic flow, in which the random degradation scenarios of CACC vehicles are taken into consideration.

The remainder of this paper is organized as follows. In the next section, the motivation of this study will be introduced. In Section 3, a generalized framework for the LWR model with such mixed vehicular flow is proposed based on the mixed fundamental diagram with different CACC penetration rates. Then in Section 4, one type of the mixed traffic flow and its degradation scenarios are described. In Section 5, three concrete surrogate car-following models are selected as an example to study the propagation of small perturbations and shock waves along the mixed platoon. Some discussions are provided in Section 6. Finally, conclusions are summarized in Section 7.

2. Motivation

It has been pointed out that an exclusive lane for CACC vehicles will be achieved in the future (Zhong and Lee 2019, Rad et al. 2020). Then the traffic scenario of a highway will consist of the CACC exclusive lane and regular lanes. Because speeds of CACC vehicles are desired to be higher than those of manual vehicles, the CACC exclusive lane will be the fast lane. Based on the knowledge we have now about traffic operations of CACC vehicles, we could define driving rules of the exclusive lane and regular lanes. The exclusive lane is designed for CACC vehicles. It only allows access for CACC vehicles running on the exclusive lane. Manual vehicles can only run on regular lanes. Moreover, CACC vehicles can also run on regular lanes if it is less congested in the regular lanes than the CACC exclusive lane.

Based on two-pipe theory proposed by Daganzo (2002), we can analyze different scenarios about the traffic system with CACC exclusive lane. To deal with this, a graph here is helpful to understand this phenomenon, as shown in Figure 1.

In Figure 1, v_{01} denotes free flow speed of CACC vehicles on the exclusive lane, whereas v_{02} stands for that of manual vehicles on the regular lane. In light traffic, as shown in Figure 1(a), all CACC vehicles run on the exclusive lane, whereas all manual vehicles run on the regular lane. Traffic streams of CACC vehicles and manual vehicles are separate and have different speeds, which is the two-pipe phenomenon described in Daganzo (2002). For such a case, the original LWR model can be used to describe traffic characteristics of these two separate streams of CACC and manual vehicles on different lanes.

As shown in Figure 1(b), when traffic density increases, the speed of CACC vehicles on the exclusive lane decreases and so does the spacing. If their speeds on the exclusive lane are lower than the free flow speed of manual vehicles, that is, 120 km/hr, which denotes a critical point, some CACC vehicles would take lane-changing behaviors to run on regular lanes. This phenomenon corresponds to the transition from two-pipe regimes to a one-pipe regime (Daganzo 2002). Meanwhile, traffic of the regular lanes will become the mixed flow. When speeds of all lanes become almost the same, the mixed traffic will achieve a synchronized flow state, as shown in Figure 1(c), in which v_s denotes the speed of synchronized flow. Then there will be no lane-changing behaviors in the mixed traffic. This is the one-pipe phenomenon described in Daganzo (2002). In this case, traffic characteristics of homogenous CACC vehicular flow on the exclusive lane can be analyzed by the original LWR model. However, the regular lane's traffic is mixed flow with CACC vehicles and manual vehicles, and a new model needs to be proposed to analyze traffic characteristics of such a mixed flow. Then this paper is motivated to propose a new LWR model for such mixed synchronized flow on the regular lane with different CACC penetration rates.

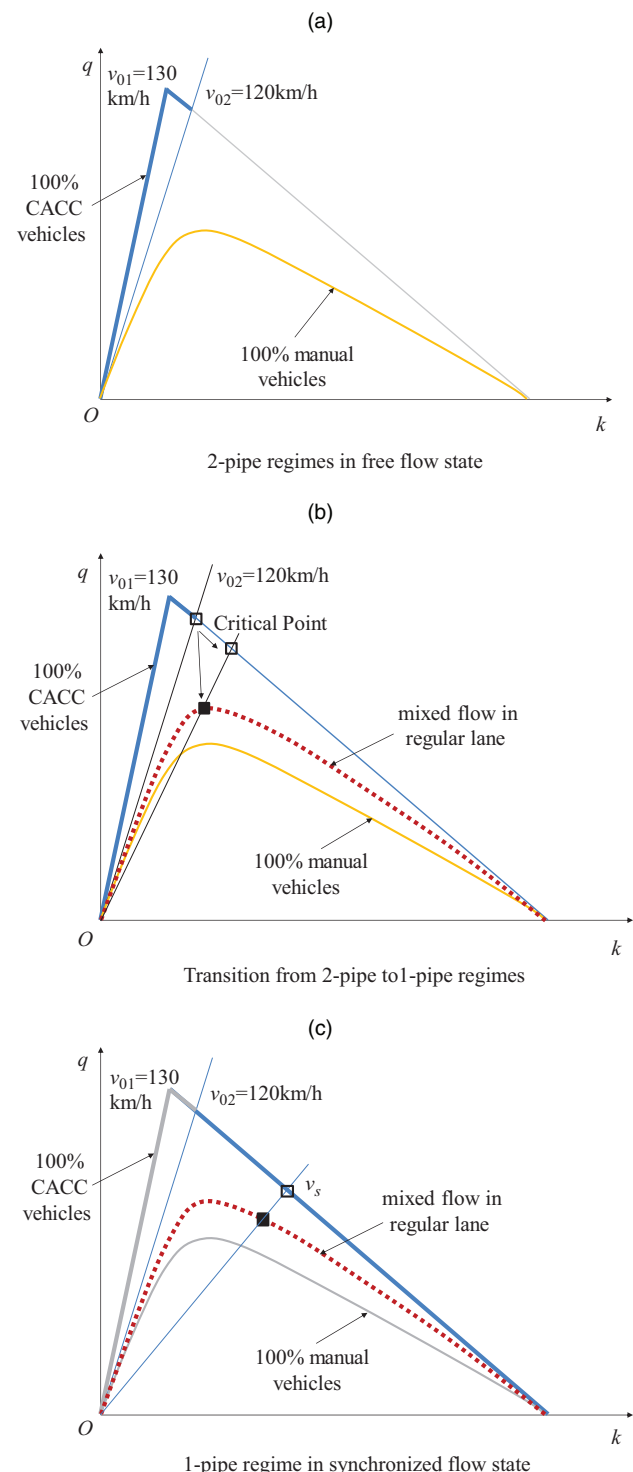
3. LWR Model of the Mixed Traffic Flow

The LWR model (Lighthill and Whitham 1955, Richards 1956) can be expressed as follows:

$$\begin{cases} \frac{\partial k}{\partial t} + \frac{\partial q}{\partial x} = 0 \\ q = kv \\ v = V(k) \end{cases}, \quad (1)$$

where $\partial k / \partial t$ is partial differential of density k with respect to time t , and $\partial q / \partial x$ is partial differential of flow

Figure 1. (Color online) One-Pipe and Two-Pipe Regimes Theory



Notes. (a) Two-pipe regimes in free flow state. (b) Transition from two-pipe to one-pipe regimes. (c) One-pipe regime in synchronized flow state.

q with respect to space x . The expression $v = V(k)$ is the fundamental diagram, which should meet

$$\frac{dq}{dk} = u, \quad (2)$$

where dq/dk is the derivative of flow q with respect to density k at equilibrium, and u is the kinematic wave speed relative to the road.

3.1. Fundamental Diagram of Mixed Traffic Flow

In mixed vehicular flow, all cars run with the same speed at equilibrium but with different spacings determined by respective car-following laws. For generalized investigation, we use h_m , h_a , and h_c as the equilibrium spacings of manual vehicles, ACC vehicles, and CACC vehicles, respectively. Assume that the mixed traffic flow contains N vehicles, which are randomly interspersed on a single lane, and that a CACC vehicle degrades to an ACC vehicle if V2V communications are not available. All cars run with the same speed at equilibrium. Hence, the length of the entire mixed traffic flow can be calculated by summing each car's equilibrium spacing as follows:

$$L = Np_m h_m + Np_a h_a + Np_c h_c, \quad (3)$$

where L is the length of the entire mixed traffic flow, and p_m , p_a , and p_c denote the expected proportions of manual, ACC, and CACC vehicles, respectively, after the degradation from CACC to ACC, which will be expressed using the original CACC penetration rate in the rest of the paper.

Based on the definition of density, the mixed traffic flow density k is obtained:

$$k = \frac{1}{Np_m h_m + Np_a h_a + Np_c h_c}. \quad (4)$$

In Equation (4), the equilibrium spacings, namely, h_m , h_a , and h_c , are functions of equilibrium speeds. The expected proportions of the three types of vehicles, namely, p_m , p_a , and p_c , are determined by the original CACC penetration rate. Therefore, Equation (4) is considered the fundamental diagram of the mixed vehicular flow under different original CACC penetration rates.

3.2. Kinematic Wave Speed of the Mixed Traffic Flow

Based on the requirement of the LWR model theory, the derivative of flow with respect to density at equilibrium should be the kinematic wave speed, which is described by Equation (2). Therefore, in the case of mixed traffic flow, it needs to be proven that the tangent slope of the mixed fundamental diagram at a macroscopic level should be equal to the kinematic wave speed propagating through the mixed platoon. Only then can we use the mixed fundamental diagram obtained in Equation (4) to present the LWR model for the mixed flow scenarios, where ACC is considered as an alternative fallback option of the CACC system when V2V communications are not available.

3.2.1. Kinematic Wave Speed at the Macroscopic Level. In order to build a general derivation framework, we obtained the density of the mixed traffic flow in Equation (4). Therefore, flow q is described as a function of speed v :

$$q = \frac{v}{p_m h_m + p_a h_a + p_c h_c}. \quad (5)$$

The derivative of flow q with respect to density k , namely, dq/dk , can be calculated using

$$\frac{dq}{dk} = \frac{dq}{dv} \frac{dv}{dk}, \quad (6)$$

where dq/dv is the derivative of q with respect to v , and dv/dk is the derivative of v with respect to k . The expression of dq/dv can be directly calculated using Equation (5), as follows:

$$\frac{dq}{dv} = \frac{(p_m h_m + p_a h_a + p_c h_c) - v(p_m h_m^v + p_a h_a^v + p_c h_c^v)}{(p_m h_m + p_a h_a + p_c h_c)^2}, \quad (7)$$

where h_m^v , h_a^v , and h_c^v are, respectively, derivatives of h_m , h_a , and h_c with respect to v .

Taking the derivative of both sides of Equation (4) with respect to density k gives

$$\frac{dv}{dk} = \frac{-(p_m h_m + p_a h_a + p_c h_c)^2}{p_m h_m^v + p_a h_a^v + p_c h_c^v}. \quad (8)$$

Substitute Equation (7) and Equation (8) into Equation (6) to obtain the derivative of flow with respect to density:

$$\frac{dq}{dk} = \frac{v(p_m h_m^v + p_a h_a^v + p_c h_c^v) - (p_m h_m + p_a h_a + p_c h_c)}{p_m h_m^v + p_a h_a^v + p_c h_c^v}. \quad (9)$$

3.2.2. Kinematic Wave Speed at the Microscopic Level.

For both backward kinematic waves and forward kinematic waves, the time that a kinematic wave takes to travel between two adjacent vehicles was derived as follows (Holland 1998):

$$\tau = \frac{h}{v - c} = [V'(h)]^{-1}, \quad (10)$$

where τ is the kinematic wave travel time between the two vehicles, h is the equilibrium spacing, v is the equilibrium speed, c is the kinematic wave speed between these two vehicles relative to the road, and $V(h)$ denotes the equilibrium speed-spacing function. The kinematic wave is called a backward wave if c is negative and is called a forward wave when c is positive.

Based on Holland (1998), the total time the kinematic wave takes to pass through a platoon is calculated as follows:

$$T_{total} = \sum_{i=1}^N \tau_i = \sum_{i=1}^N [V'_i(h)]^{-1}, \quad (11)$$

where i denotes the i th vehicle, and N is the total number of vehicles.

Because spacing h is the function of speed v at equilibrium, it can be described as follows:

$$\begin{cases} h = f(v) \\ v = V(h) \end{cases}. \quad (12)$$

For $h = f(v)$, taking the derivative of both sides with respect to spacing h gives

$$1 = \frac{df}{dv} \frac{dv}{dh} = h^v V'(h). \quad (13)$$

Therefore, we can obtain that

$$\begin{cases} [V'_m(h)]^{-1} = h_m^v \\ [V'_a(h)]^{-1} = h_a^v \\ [V'_c(h)]^{-1} = h_c^v \end{cases}, \quad (14)$$

where the subscript m , a , and c denotes manual, ACC, and actual CACC vehicles, respectively.

Substitute Equation (14) into Equation (11) to obtain the total time the kinematic wave takes to pass through a mixed platoon:

$$T_{total} = N(p_m h_m^v + p_a h_a^v + p_c h_c^v). \quad (15)$$

During the time of T_{total} , the kinematic wave propagates from the leading car to the last car in the platoon. Then, the displacement the kinematic wave travels relative to the road is calculated:

$$D = x_{last}(t + T_{total}) - x_{lead}(t), \quad (16)$$

where $x_{last}(t + T_{total})$ denotes the position of the last vehicle in the platoon at the time of $(t + T_{total})$, and $x_{lead}(t)$ is the position of the leading car at the time of t .

Because the platoon is traveling at the equilibrium speed at t moment, the length of the entire mixed flow described in Equation (3) at equilibrium is $x_{lead}(t) - x_{last}(t)$. During the time of T_{total} , the displacement of the last car is $x_{last}(t + T_{total}) - x_{last}(t) = v T_{total}$. Then, the value of D can be obtained by subtracting the length of the entire mixed traffic flow from the distance that the last vehicle runs during the time of T_{total} , as follows:

$$\begin{aligned} D &= [x_{last}(t + T_{total}) - x_{last}(t)] - [x_{lead}(t) - x_{last}(t)] \\ &= N[v(p_m h_m^v + p_a h_a^v + p_c h_c^v) - (p_m h_m + p_a h_a + p_c h_c)]. \end{aligned} \quad (17)$$

Therefore, the average kinematic wave speed propagating through the mixed traffic flow relative to the road, denoted as u , is obtained:

$$u = \frac{D}{T_{total}} = \frac{v(p_m h_m^v + p_a h_a^v + p_c h_c^v) - (p_m h_m + p_a h_a + p_c h_c)}{p_m h_m^v + p_a h_a^v + p_c h_c^v}. \quad (18)$$

It is found that the fundamental diagrams of the mixed traffic flow meet the constraint condition of Equation (2), that is, $dq/dk = u$, by comparing Equation (9) and Equation (18).

Based on the previous observations, it is analytically proven that the tangent slope of the mixed

fundamental diagram is equal to the kinematic wave speed propagating through the mixed platoon. Therefore, the fundamental diagram derived in Equation (4) can be used to present the LWR model of the mixed traffic flow studied in this paper, as follows:

$$\begin{cases} \frac{\partial k}{\partial t} + \frac{\partial q}{\partial x} = 0 \\ q = kv \\ k = \frac{1}{p_m h_m + p_a h_a + p_c h_c} \end{cases}. \quad (19)$$

4. Mixed Traffic Flow

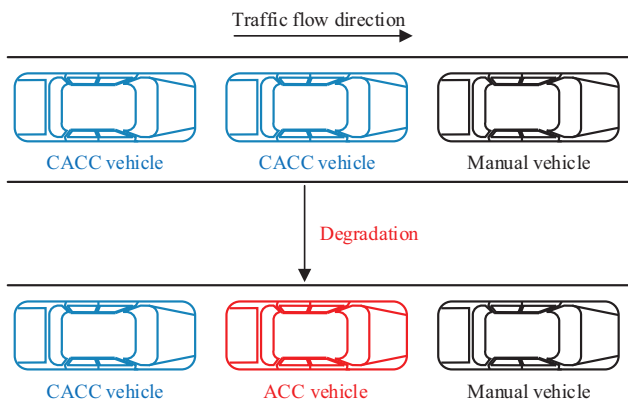
4.1. Scenario Description

Based on the design of CACC systems, there might be a need for information from multiple vehicles and in the absence of such information, the system should degrade to ACC. Then the degradation from CACC to ACC is quite complicated. However, the real experiments (Milanés and Shladover 2014, Milanés et al. 2014) indicate that the traffic scenario in which the CACC only monitors one vehicle ahead via the V2V communication is expected to be the first to come into being. Therefore, this paper focuses on the LWR model with this type mixed traffic flow. Because ACC vehicles are degraded from some CACC vehicles, to avoid confusion, nonmanual driven vehicles are all called original CACC vehicles in the rest of our paper. The degraded CACC vehicles are called ACC vehicles, whereas other non-degraded CACC vehicles are called actual CACC vehicles. Thus, original CACC vehicles contain ACC vehicles and actual CACC vehicles.

In such a randomly mixed flow, several types leading-following combinations are possible. If the following vehicle is a manual vehicle, it can only be manually driven. When the following and preceding vehicles are both CACC vehicles, the following vehicle can be driven automatically using its CACC car-following system. If the following vehicle is a CACC vehicle and the preceding vehicle is a manual vehicle, the CACC system of the following vehicle does not work because there is no V2V communication between them. Then, the following vehicle uses the ACC system as an alternative fallback option for the CACC system. This means that the CACC vehicle inherently degrades to an ACC vehicle in this case (Ploeg et al. 2015, Wang et al. 2019). When the CACC system degrades to an ACC system, the V2V communication is still working. Therefore, a CACC vehicle can still be driven automatically when following an ACC vehicle, as shown in Figure 2.

In summary, the mixed traffic flow studied in this paper is comprised of manual vehicles, CACC

Figure 2. (Color online) Degradation Scenario of Mixed Traffic Flow Studied in This Paper



vehicles, and ACC vehicles. However, ACC vehicles exist in the mixed traffic flow if and only if a CACC vehicle degrades to an ACC vehicle when following a manual vehicle, as an alternative fallback option of the CACC system.

4.2. Mathematical Expression

According to the mixed LWR model described in Equation (19), it is necessary to determine the expected proportions of the three types of vehicles, namely, p_m , p_a , and p_c , in the mixed traffic flow, using the original CACC penetration rate.

In this paper, the symbol p ($0 \leq p \leq 1$) is used to denote the original CACC penetration rate. Suppose that there are N vehicles in the mixed traffic flow; then, the number of original CACC vehicles is Np and that of manual vehicles is $N(1 - p)$. Because N is large enough in traffic flow, from a probabilistic perspective, the probability that an original CACC vehicle follows a manual vehicle is the product of their proportions, namely, $p(1 - p)$. An original CACC vehicle degrades to an ACC vehicle if and only if it follows a manual vehicle. Therefore, the probability of degradation is $p(1 - p)$. This means that the expected number of ACC vehicles is $Np(1 - p)$. Then, the expected number of actual CACC vehicles Np^2 is obtained by subtracting ACC vehicles from the original CACC vehicles. Thus, the expected proportions of the three types of vehicles are expressed by using original CACC penetration rate p , as follows:

$$\begin{cases} p_m = 1 - p \\ p_c = p^2 \\ p_a = p(1 - p) \end{cases}. \quad (20)$$

As such, Equation (20) determines the probabilities of random degradation scenarios in the mixed traffic flow. The analytical studies in the rest of this paper are based on these probabilities. Without losing

generality, Equation (20) incorporates homogeneous flow of manual vehicles if p is 0 and that of actual CACC vehicles when p equals to 1. We should note that the probabilities in Equation (20) are of statistical significance and should not be interpreted against a specific instant or pattern. This means the proportions of three types of vehicles are not fixed, whereas they denote the expectation probability from the perspective of statistical property.

5. Example Application of the Mixed Flow LWR Model

In this section, three concrete car-following models are selected as the manual, ACC, and CACC models, respectively. Based on the generalized framework presented previously, the mixed fundamental diagram and LWR model are obtained in detail for this case. Additionally, numerical simulations are also performed to illustrate the propagation of small perturbation and shock waves along the mixed platoon using the three car-following models.

5.1. Car-Following models

The CACC and ACC models validated with experimental data by the PATH program are used as the example models for real CACC vehicles and current factory ACC vehicles, respectively. The intelligent driver model (IDM) is used as the example car-following model for manually driven vehicles.

5.1.1. Manual Driven Model. IDM (Treiber, Hennecke, and Helbing 2000) is widely used for the investigation of manually driven performance because of its realistic acceleration profiles and plausible behavior in essentially all single-lane traffic situations (Treiber and Kesting 2013). The acceleration equation is written as

$$\dot{v} = a \left[1 - \left(\frac{v}{v_0} \right)^4 - \left(\frac{s_0 + vT + \frac{v\Delta v}{2\sqrt{ab}}}{h - l} \right)^2 \right], \quad (21)$$

where \dot{v} is the target acceleration of the following vehicle, a is the maximum acceleration, v is the speed of the following vehicle, v_0 is the desired speed, s_0 is the desired minimum gap distance, T is the safe time headway, Δv is the speed difference between two adjacent vehicles, b is the desired deceleration, h is the spacing, and l is the vehicle length. The model parameters determined in previous literature are used here, which are summarized in Table 1.

5.1.2. ACC Model. The ACC car-following model calibrated with experimental data by PATH (Milanés and Shladover 2014) is used in this paper. Field experiments show that this model is a good fit for the car-following dynamics of a current commercially available ACC system whose control strategy is often

Table 1. Model Parameters of the IDM

Parameters	Values	Related literature
T	1.5 seconds	Kesting et al. 2008, Kesting, Treiber, and Helbing 2010, Shladover et al. 2015
a	1 m/s ²	Treiber et al. 2000, Kesting et al. 2008, Kesting, Treiber, and Helbing 2010, Milanés and Shladover 2014
v_0	33.3 m/s	
s_0	2 m	
b	2 m/s ²	
l	5 m	

proprietary. The ACC model takes the following form:

$$\dot{v} = k_1(h - l - s_0 - t_a v) + k_2 \Delta v, \quad (22)$$

where h , l , and s_0 have the same meanings as those in Equation (21). k_1 and k_2 are control gains, and t_a is the ACC desired time gap.

To determine the values of k_1 and k_2 , an optimization criterion based on the integral absolute error (IAE) was used (Milanés and Shladover 2014). The minimum IAE was obtained when k_1 equals 0.23 s⁻² and k_2 is 0.07 s⁻². The value of time gap t_a is set at 1.1 seconds in the experiment, which is a suitable value for the commercial ACC system.

5.1.3. CACC Model. PATH proposed a CACC model by simplifying a CACC controller implemented in production vehicles (Milanés and Shladover 2014, Milanés et al. 2014). The CACC controller is divided into a gap closing stage and a gap regulation stage (Milanés et al. 2014). This paper mainly focuses on the characteristics of the LWR model at equilibrium. Therefore, the gap regulation stage is used as the CACC model in our paper, which is calculated as follows:

$$v = v_{prev} + k_p e + k_d \dot{e}, \quad (23)$$

where v_{prev} is the following vehicle speed in the previous iteration, k_p and k_d are control gains, and e denotes the gap distance error calculated as follows:

$$e = h - l - s_0 - t_c v, \quad (24)$$

where t_c is CACC desired time gap, which is set as 0.6 seconds during experimental tests.

The values of k_p and k_d are determined based on the CACC implementation (Milanés and Shladover 2014, Milanés et al. 2014), where k_p is equal to 0.45 and k_d is equal to 0.25. The experimental tests show that the CACC model properly matches the real car-following behavior of the production CACC vehicles.

5.2. Fundamental Diagram and LWR Model

5.2.1. Homogenous Traffic Flow. In homogenous traffic flow, all cars have the same speed and the same spacing at equilibrium. Equilibrium conditions can be described as follows:

$$\begin{cases} \dot{v} = 0 \\ \Delta v = 0 \end{cases} \quad (25)$$

The equilibrium spacing of IDM under the condition of Equation (25) can be described as a function of equilibrium speed. Thus,

$$h_m = \frac{s_0 + T v}{\sqrt{1 - (v/v_0)^4}} + l, \quad (26)$$

where h_m is the spacing of manual vehicles at equilibrium, v is the equilibrium speed, and others are IDM parameters.

The spacing h_m can be translated into the density k by taking its reciprocal:

$$k = \frac{1}{h_m}. \quad (27)$$

Therefore, the fundamental diagram of manual vehicles can be obtained, as follows:

$$\begin{cases} k = \frac{\sqrt{1 - (v/v_0)^4}}{s_0 + vT + l\sqrt{1 - (v/v_0)^4}}, \\ q = kv \end{cases} \quad (28)$$

where q is the flow, and only the density k as a function of speed v can be solved analytically. Therefore, its q - k fundamental diagram can be obtained numerically using parametric plots with various speed v (Kesting and Treiber 2008).

For the ACC vehicles, substitute Equation (25) into the ACC model to obtain the equilibrium spacing of ACC vehicles, as follows:

$$h_a = t_a v + l + s_0, \quad (29)$$

where h_a is the spacing of ACC vehicles at equilibrium. Based on the relationship between spacing and density, the fundamental diagram of ACC vehicles can be obtained as follows:

$$q = \frac{1 - (l + s_0)k}{t_a}, \quad (30)$$

where flow q can be analytically described as a function of density k . Thus, its fundamental diagram can be directly calculated based on Equation (30).

Finally, the equivalents of actual CACC vehicles can also be obtained by this way, as follows:

$$h_c = t_c v + l + s_0, \quad (31)$$

$$q = \frac{1 - (l + s_0)k}{t_c}, \quad (32)$$

where h_c is the equilibrium spacing of actual CACC vehicles. Equation (32) is the fundamental diagram of actual CACC vehicles. In addition, CACC and ACC vehicles can have larger free-flow speed, which is set as about 130 km/hr in this paper.

Based on the previous observations, the homogeneous fundamental diagrams of the three types of vehicles are calculated, as shown in Figure 3. Figure 3 shows that the fundamental diagrams of ACC and actual CACC vehicles only have congested region without free-flow region. This is because the ACC and CACC models were validated using experimental data by PATH (Milanés and Shladover 2014) to describe only car-following region. If necessary, we may add a line to represent the free-flow region on the fundamental diagrams, for example, the black dashed line in Figure 4.

5.2.2. Mixed Traffic Flow. The generalized density of mixed traffic flow was obtained in Equation (4). The expected proportions of the three types of vehicles in the mixed platoon are determined by the original CACC penetration rate p in Equation (20). The spacings of the three selected car-following models are taken into consideration, namely, substituting Equation (20), Equation (26), Equation (29), and Equation (31) into Equation (4) yields

$$k = \frac{1}{(1-p)\left(\frac{s_0+Tv}{\sqrt{1-(\frac{v}{v_0})^4}} + l\right) + p(1-p)(t_a v + s_0 + l) + p^2(t_c v + s_0 + l)}. \quad (33)$$

Equation (33) shows that density k as a function of speed v can be solved analytically but the inverse cannot. Therefore, the q - k fundamental diagram of the mixed traffic flow can be obtained numerically by

Figure 3. (Color online) Homogenous Fundamental Diagrams

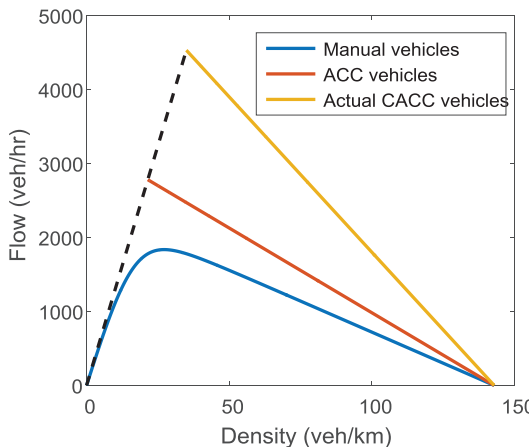
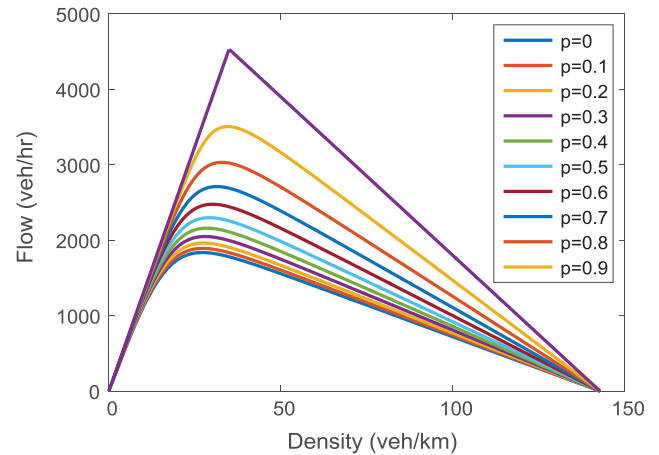


Figure 4. (Color online) Fundamental Diagram of the Mixed Traffic Flow



parametric plots varying speed v (Kesting and Treiber 2008), as shown in Figure 4.

Figure 4 indicates that the capacity of the mixed traffic flow increases as p increases. Based on the generalized framework of the mixed LWR model presented previously, substituting Equation (33) into Equation (1) yields

$$\begin{cases} \frac{\partial k}{\partial t} + \frac{\partial q}{\partial x} = 0 \\ q = kv \\ k = \frac{1}{(1-p)\left(\frac{s_0+Tv}{\sqrt{1-(\frac{v}{v_0})^4}} + l\right) + p(1-p)(t_a v + s_0 + l) + p^2(t_c v + s_0 + l)} \end{cases}. \quad (34)$$

Equation (34) is the mixed flow LWR model when the three types of car-following models are selected as those in Section 5.1. Because the parameters of the car-following models are fixed, the equilibrium properties of the mixed LWR model are determined by both equilibrium speed v and original CACC penetration rate p .

5.3. Numerical Simulations

The car-following models in Equation (21) through Equation (23), namely, the IDM model and the ACC/CACC models proposed by PATH, are used in simulations. The random degradation scenarios of CACC vehicles are also considered based on Figure 2.

5.3.1. Propagation of Small Perturbation. Taking the car-following models selected in Section 5.1 into consideration, their equilibrium spacings h_m , h_a , and h_c have been obtained in Equation (26), Equation (29), and Equation (31), respectively. The derivatives with

respect to speed, namely, h_m^v , h_a^v , and h_c^v , can then be calculated, as follows:

$$\left\{ \begin{array}{l} h_m^v = \frac{T\sqrt{1 - (v/v_0)^4} + (s_0 + Tv)\frac{2v^3}{v_0^4}\frac{1}{\sqrt{1 - (v/v_0)^4}}}{1 - (v/v_0)^4} \\ h_a^v = t_a \\ h_c^v = t_c \end{array} \right. . \quad (35)$$

We rewrite the generalized kinematic wave speed expression in Equation (9) or Equation (18), by bringing all model parameters, as follows:

$$\frac{dq}{dk} = u = \frac{v(1-p)\frac{Tv_0^4[1 - (v/v_0)^4] + 2v^3(s_0 + Tv)}{v_0^4[1 - (v/v_0)^4]^{3/2}} - (1-p)[-\frac{s_0 + Tv}{\sqrt{1 - (v/v_0)^4}} + l] - p(s_0 + l)}{(1-p)\frac{Tv_0^4[1 - (v/v_0)^4] + 2v^3(s_0 + Tv)}{v_0^4[1 - (v/v_0)^4]^{3/2}} + pt_a + p^2(t_c - t_a)}. \quad (36)$$

This shows that we can calculate the values of kinematic wave speed for a certain equilibrium speed under different original CACC penetration rates based on Equation (36). In order to obtain both forward and backward kinematic wave speeds, 30 and 15 m·s⁻¹ are selected to be equilibrium speeds. Then the analytical values of kinematic wave speed under different values of p are calculated, as shown in Table 2.

For comparison and verification purpose, numerical simulations are also performed with these two equilibrium speeds. The simulations focus on a mixed traffic platoon consisting of 100 vehicles. The numbers of original CACC vehicles and manual vehicles are determined randomly based on the original CACC penetration rate predetermined for each simulation. These two types of vehicles are interspersed randomly on a single lane. Then, the original CACC vehicle degrades to an ACC vehicle if it follows a manual vehicle. All

cars move with the same equilibrium speed in the initial state, and each car has its equilibrium spacing based on its car-following law. The equilibrium will be disturbed when a small perturbation is added onto the leading vehicle, which decelerates by $-0.5 \text{ m}\cdot\text{s}^{-2}$ for two seconds and then keeps the speed until the end of the simulation. The simulation time step is 0.01 seconds.

We focus on the kinematic wave speed in the simulations. The time taken by the kinematic wave to pass through the mixed traffic flow is the span from the moment when the small perturbation lasts for one second to the moment when the last vehicle decreases by $0.5 \text{ m}\cdot\text{s}^{-1}$. During this time, the displacement that the kinematic wave travels relative to the road is calculated based on the positions of the head and tail vehicles. Then, the simulation values of kinematic wave speed can be obtained. Additionally, in order to account for the effect of randomness, each simulation was repeated 10 times. The simulation values of kinematic wave speed for each value of p were calculated based on the average of the results from 10 simulations, as shown in Table 2.

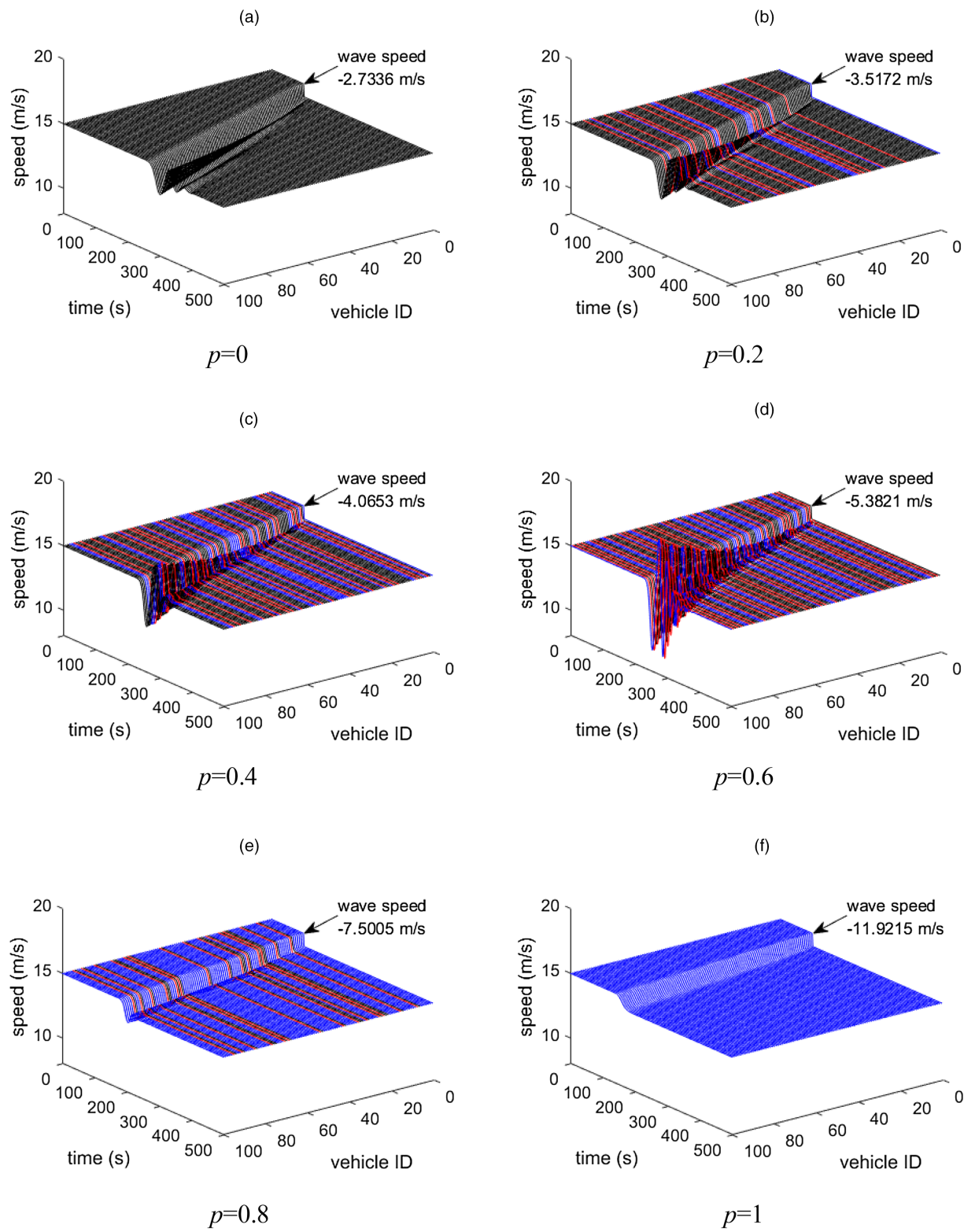
It is found that the forward kinematic wave propagates through the mixed platoon when the equilibrium speed is equal to 30 m·s⁻¹, whereas the backward kinematic wave propagates upstream if the equilibrium speed is 15 m·s⁻¹, except for the case in which p is 1. The kinematic wave is always the backward wave when p equals 1, because the fundamental diagram of the CACC model only has the congested density range. More importantly, the simulation results are almost consistent with those of analytical calculations.

In addition, simulation speeds of each car are obtained during the time when the small perturbation propagates through the mixed platoon, as shown in Figure 5. The initial equilibrium speed is 15 m·s⁻¹ in Figure 5. Each line denotes speed dynamics of every vehicle in the mixed flow. The simulation values of

Table 2. Analytical and Simulation Values of Kinematic Wave Speed

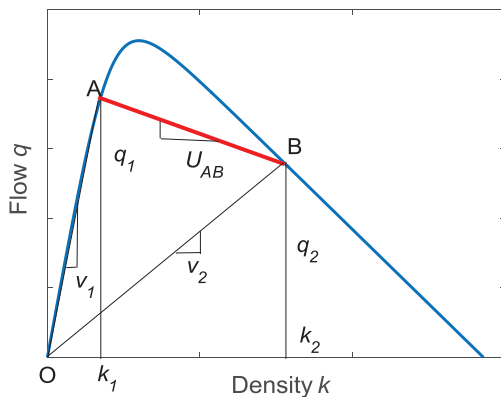
Original CACC penetration rate	Equilibrium speed: 30 m/s		Equilibrium speed: 15 m/s	
	Analytical kinematic wave speeds (m/s)	Simulation kinematic wave speeds (m/s)	Analytical kinematic wave speeds (m/s)	Simulation kinematic wave speeds (m/s)
$p = 0$	23.3863	23.3801	-2.9215	-2.7336
$p = 0.1$	23.1173	23.1132	-3.1653	-3.0262
$p = 0.2$	22.8095	22.8180	-3.4511	-3.5172
$p = 0.3$	22.4468	22.5142	-3.7910	-3.6294
$p = 0.4$	22.0033	22.2122	-4.2022	-4.0653
$p = 0.5$	21.4344	21.4558	-4.7102	-4.5895
$p = 0.6$	20.6553	20.5924	-5.3542	-5.3821
$p = 0.7$	19.4883	19.1710	-6.1975	-6.2899
$p = 0.8$	17.4399	17.0645	-7.3504	-7.5005
$p = 0.9$	12.7416	12.2105	-9.0223	-9.2395
$p = 1$	-11.6667	-12.0309	-11.6667	-11.9215

Figure 5. (Color online) Propagation of Small Perturbation Along Platoon



Notes. (a) $p = 0$. (b) $p = 0.2$. (c) $p = 0.4$. (d) $p = 0.6$. (e) $p = 0.8$. (f) $p = 1$.

Figure 6. (Color online) Diagram of Shock Wave Speed



kinematic wave speeds are also illustrated in Figure 5. It can be found that, the larger the backward kinematic wave speed is, the less the time taken by the small perturbation to reach the last car will be. This time delay decreases with the increase of original CACC penetration rate p .

5.3.2. Shock Waves. An important feature of LWR model is the representation of shock wave. The shock wave speeds under different original CACC penetration rate p are analytically calculated. Numerical simulations are also performed using car-following models.

Assume that point A denotes a traffic state, whereas point B denotes another one, as shown in Figure 6. Their traffic states are (q_1, k_1, v_1) and (q_2, k_2, v_2) , respectively. The mixed flow LWR model has been obtained in Equation (34) when the three types of car-following models are selected in Section 5.1. Thus, the shock wave speed between traffic states A and B can be calculated as follows:

$$U_{AB} = \frac{q_1 - q_2}{k_1 - k_2}, \quad (37)$$

Table 3. Shock Wave Speeds in Case 1

Original CACC penetration rate	Platoon speed: from 110 to 80 km/hr			
	Analytical shock wave speeds (km/hr)	Simulation shock wave speeds (km/hr)	Absolute error (km/hr)	Relative error (%)
$p = 0$	48.7727	48.4715	-0.3012	-0.62
$p = 0.1$	47.1741	46.9718	-0.2023	-0.43
$p = 0.2$	45.3758	44.6654	-0.7104	-1.57
$p = 0.3$	43.2994	43.4597	0.1603	0.37
$p = 0.4$	40.8227	40.7375	-0.0852	-0.21
$p = 0.5$	37.7444	37.9387	0.1943	0.51
$p = 0.6$	33.7078	33.0857	-0.6221	-1.85
$p = 0.7$	28.0139	26.2788	-1.7351	-6.19
$p = 0.8$	19.0806	16.4401	-2.6405	-13.84
$p = 0.9$	2.4025	1.5259	-0.8766	-36.49
$p = 1$	-42.0000	-44.7770	-2.7770	6.61

where U_{AB} is the analytical value of shock wave speed.

The flow q and density k of the mixed flow both depend on the speed v and original CACC penetration rate p . Therefore, the shock wave speed of the mixed traffic flow is determined by the values of v and p . In order to obtain the value ranges of shock wave speeds as fully as possible, two cases are selected. In the first case, the traffic flow speeds are, respectively, $v_1 = 110$ km/hr and $v_2 = 80$ km/hr, whereas $v_1 = 90$ km/hr and $v_2 = 60$ km/hr in the second case. The analytical shock wave speeds under different values of p are calculated for the two cases, as shown in Tables 3 and 4, respectively.

Numerical simulations are also performed to form shock waves in the mixed traffic flow with 100 vehicles, in which the original CACC vehicle degrades to an ACC vehicle if following a manual vehicle. In a real traffic scenario, shock waves are usually caused by sudden deceleration within a short period of time. Therefore, in the first case, all vehicles travel at 110 km/hr and the leading car suddenly decelerates at a rate of $-4 \text{ m}\cdot\text{s}^{-2}$ to 80 km/hr to form shock waves. In the second case, the leading vehicle decreases from 90 to 60 km/hr using the same deceleration rate as the first case. The simulation time step is also 0.01 seconds. Each simulation was repeated 10 times to account for randomness and find the average simulation values of shock wave speed. The average values obtained by the simulations are also shown in Tables 3 and 4. Additionally, the relative errors of simulation values with respect to analytical values are calculated.

The results show that most relative errors under different values of p are below or only slightly larger than about 5%. The randomness is apt to account for the errors because the analytical values of shock wave speeds are calculated based on the expected situation. The error increases to about 30% when p equals 0.9 in Table 3, and when p is 0.5 in Table 4. This is mainly

Table 4. Shock Wave Speeds in Case 2

Original CACC penetration rate	Platoon speed: from 90 to 60 km/hr			
	Analytical shock wave speeds (km/hr)	Simulation shock wave speeds (km/hr)	Absolute error (km/hr)	Relative error (%)
$p = 0$	11.3234	11.3677	0.0443	0.39
$p = 0.1$	9.6968	9.5399	-0.1569	-1.62
$p = 0.2$	7.8995	7.9160	0.0165	0.21
$p = 0.3$	5.8665	5.8572	-0.0093	-0.16
$p = 0.4$	3.5026	3.5409	0.0383	1.09
$p = 0.5$	0.6633	0.4981	-0.1652	-24.91
$p = 0.6$	-2.8846	-2.9414	-0.0568	1.97
$p = 0.7$	-7.5436	-7.7386	-0.1950	2.58
$p = 0.8$	-14.0762	-14.0900	-0.0138	0.10
$p = 0.9$	-24.1245	-27.2900	-3.1655	13.12
$p = 1$	-42.0000	-44.6457	-2.6457	6.30

because the speed values of shock waves are close to zero in those cases, where the shock wave is transforming from positive to negative. A small numerical difference near zero could easily cause a large relative error. Therefore, the absolute error should also be considered. It can be calculated that the absolute errors are -0.8766 km/hr (about -0.24 m/s) and -0.1652 km/hr (about 0.05 m/s), respectively, when p is 0.9 in Table 3 and 0.5 in Table 4. Therefore, this indicates that the proposed LWR model is effectively able to describe shock wave propagation through the mixed traffic flow studied in this paper.

In addition, the speeds of each car when the shock wave passes through the mixed platoon are also obtained in the simulations. For example, Figure 7 shows the case in which the platoon decreases from 90 to 60 km/hr. The simulation values of shock wave speeds are also illustrated in Figure 7. It can be found that there is also a time delay before shock waves reach the last car. This delay decreases with small positive shock wave speeds and large negative shock wave speeds. Therefore, the time delay is decreasing when CACC vehicles are gradually increasing. The mixed traffic flow may be able to support the shock waves for some equilibrium speeds and values of p , which leads to the stable traffic flow. However, for some other states, the mixed traffic flow would become unstable when the shock waves pass through the platoon (Treiber and Kesting 2013).

6. Discussion

The LWR model of the mixed traffic flow has been obtained above. In this section, we apply the mixed LWR model to solve some traffic flow problems, such as the queue caused by a traffic accident and the impact of a moving bottleneck (Ni 2015). Then, the performance of the mixed LWR model will be compared with simulations of the three types of car-following models. Additionally, our mixed LWR

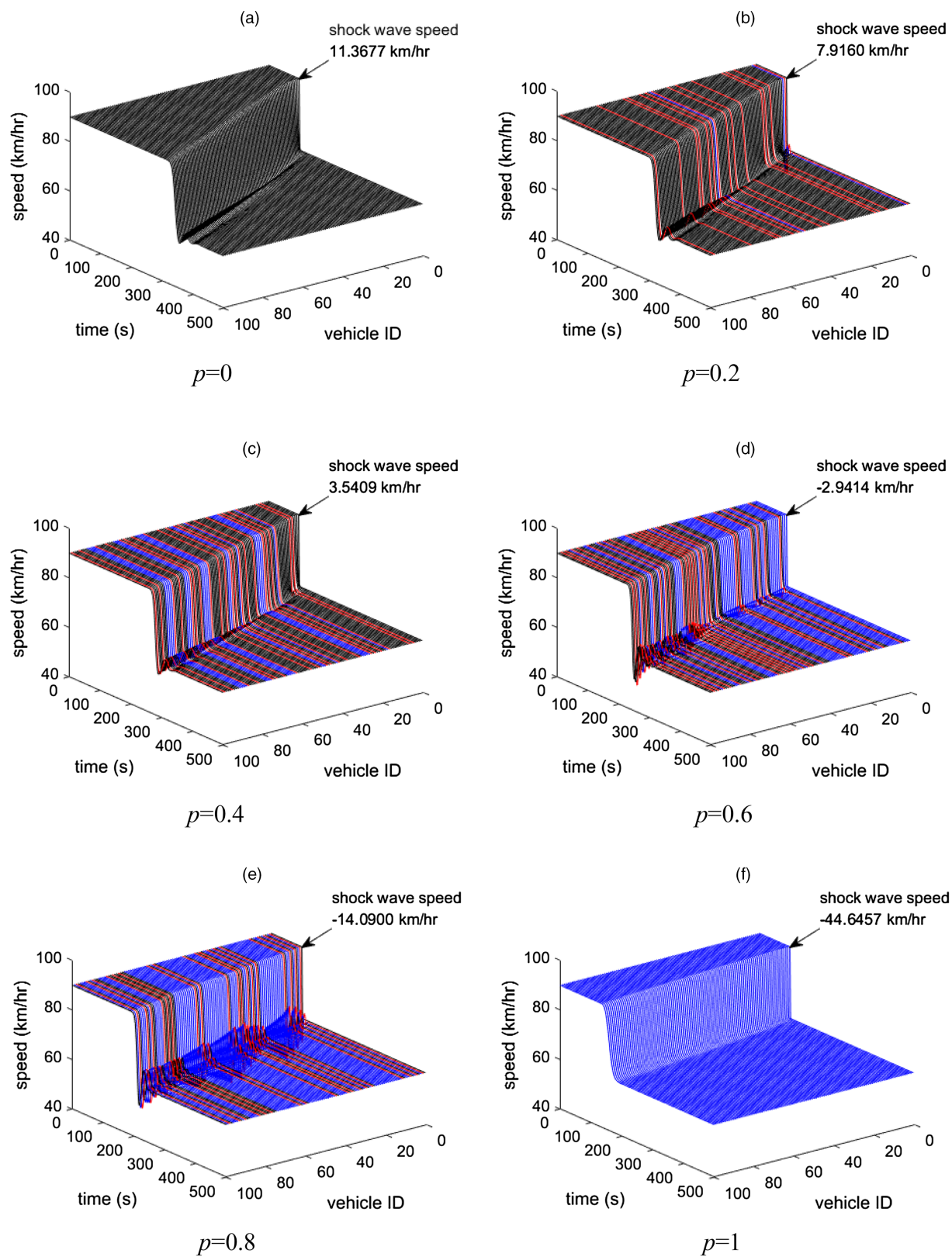
model is compared with the multiclass LWR model in these two traffic problems.

6.1. Queue Caused by a Traffic Accident

In daily traffic flow, a queue is often caused by an accident. Assume that there is an accident on one interstate. The traffic operation center then decides to completely close access to the interstate for some period of time to clean up the accident. Following cleanup, the interstate will be reopened for normal operation. In case of the mixed vehicular flow, the arrival flow is fixed. One of the concerns here is how long the queue will spill back under different CACC penetrations.

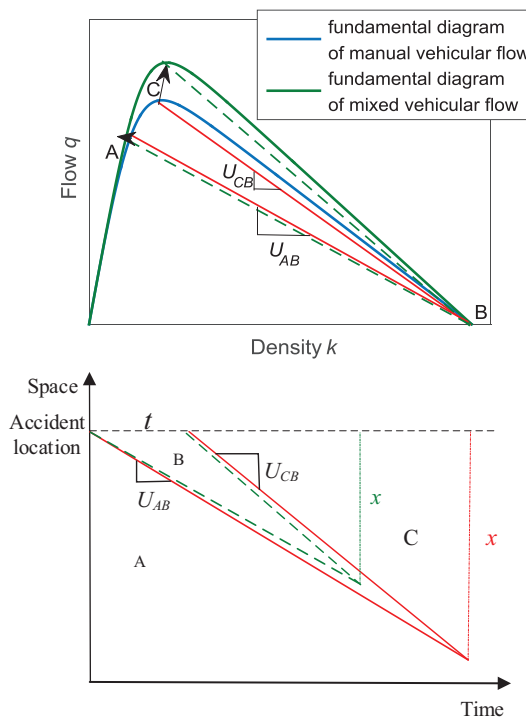
Figure 8 illustrates the graphical construction based on the LWR theory to calculate the queue length. In Figure 8, condition A denotes the arrival flow, condition B is the queue flow when the interstate is shut off, and condition C is the capacity flow. U_{AB} is the shock wave speed cased by arrival flow and queue flow during the closure of the Interstate. U_{CB} denotes the shock wave speed caused by queue flow and capacity flow when the interstate is reopened. The line segment t in the time axis denotes the time during which the interstate is shut off, whereas the line segment x in the space axis is the queue length caused by the accident. Based on the mixed fundamental diagram obtained in Figure 4 in Section 5, the fundamental diagram curve moves up and out with the increase of CACC penetration rate. Moreover the free flow region of the CACC model is assumed to be a line, as can be seen in Figure 4. Therefore, condition A moves left and condition C moves up when CACC penetration rate increases, which is illustrated using the dashed line in Figure 8. It can be seen that both A and C move in directions that shorten the queue length x . Thus, CACC can always improve the queue.

Figure 7. (Color online) Propagation of Shock Waves Along Platoon



Notes. (a) $p = 0$. (b) $p = 0.2$. (c) $p = 0.4$. (d) $p = 0.6$. (e) $p = 0.8$. (f) $p = 1$.

Figure 8. (Color online) Graphical Construction of Queue Length



Based on the graphical construction in Figure 8, the queue length for each CACC penetration rate can be calculated as follows:

$$x = \frac{t|U_{AB}| |U_{CB}|}{|U_{CB}| - |U_{AB}|}, \quad (38)$$

where $|\cdot|$ denotes the absolute value. As mentioned previously, shock wave speeds of the mixed LWR for certain conditions are determined by CACC penetration rates. Therefore, the queue length x under different CACC penetration rates can be obtained based on the mixed LWR model derived in this paper.

Here, the arrival flow is fixed at 1,500 vehicles/hr, and the cleanup time t is assumed as 15 minutes. Then, the results of queue length are shown in Table 5. It can be clearly seen that the queue length decreases with the increase of CACC penetration rate. In particular, the queue can be improved by 64.66% when CACC penetration rate increases to one.

6.2. Impact of a Moving Bottleneck

The sluggish truck on a freeway is another traffic flow problem known as a moving bottleneck. A freeway is initially operating under certain condition. Then, a sluggish truck enters the freeway at a low speed. Shortly, the truck turns off the freeway at the next exit. Our interest is the impact duration of the truck under different CACC penetration rates.

The graphical construction for this problem is shown in Figure 9 where condition **A** is the initial operation condition of the freeway, whereas condition **B** denotes the traveling speed of the truck. Condition **C** is the capacity condition when the truck turns off the freeway. U_{OB} is the truck traveling speed, whereas U_{AB} is the shock wave speed caused by conditions **A** and **B** when the arrival vehicular flow travels behind the truck. Furthermore, U_{CB} is the shock wave speed caused by condition **C** and **B** when the truck turns off the freeway. The line segment S in the space axis is the distance the truck travels, and the line segment t in the time axis is the duration of impact of the truck. The fundamental diagram curve obtained in Section 5 moves up and out with the increase of CACC penetration rate. Because the arrival flow and the truck speed are assumed to be constant for the mixed vehicular flow, condition **A** moves left, and both conditions **B** and **C** move up with the increase of CACC penetration rate, as shown using the dashed line in Figure 9. As indicated, both **B** and **C** move in directions that reduce the duration of impact, whereas the motion of **A** increases the duration of impact. Therefore, the influence of CACC depends on the conditions of **A**, **B**, and **C** when the mixed fundamental diagram is determined. Based on the graphical construction, the duration of impact of the truck under different CACC penetration rates can be calculated as follows:

$$t = \frac{S(U_{OB} + |U_{CB}|)}{U_{OB}(U_{AB} + |U_{CB}|)}, \quad (39)$$

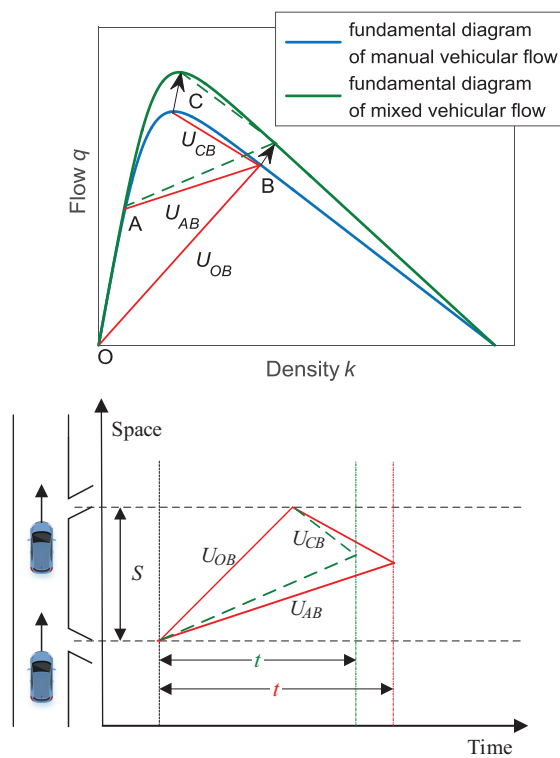
where $|\cdot|$ denotes absolute value. The shock wave speeds for each CACC penetration rate can be calculated using the mixed LWR model proposed in this paper. Thus, the duration of impact of the truck can be obtained under different CACC penetration rates.

Here, the arrival flow of condition **A** is fixed as 1,000 vehicles/hr, the truck speed of condition **B** is assumed to be 50 km/hr, and the distance S traveled by the truck is 10 km. The durations of impact are calculated and shown in Table 6. It is shown that the duration of

Table 5. Queue Length for Different CACC Penetration Rates

CACC penetration rate p	Queue length (km)	Reduced (%)
$p = 0$	11.2130	—
$p = 0.1$	10.2298	8.77
$p = 0.2$	9.2908	17.14
$p = 0.3$	8.3867	25.21
$p = 0.4$	7.5552	32.62
$p = 0.5$	6.7884	39.46
$p = 0.6$	6.1077	45.53
$p = 0.7$	5.5072	50.89
$p = 0.8$	4.9995	55.41
$p = 0.9$	4.5219	59.67
$p = 1$	3.9628	64.66

Figure 9. (Color online) Graphical Construction of the Time of Impact



impact reduces with the increase of CACC penetration rates, although the percent reduction is relatively small. If the CACC penetration rate reaches one, the duration of impact can only be reduced by 28.54%.

6.3. Comparison with Simulations of Car-Following Models

Generally speaking, one key analysis for traffic flow problems described previously is the analysis of the accuracy of the proposed mixed LWR model compared with microscopic simulation models. Therefore, the consistency between the analytical results of the mixed LWR model and the simulation results of the car-following models is further studied.

The three car-following models selected in our example are used in simulations, which are performed under different CACC penetration rates, and the relative space positions of vehicles are random. The simulation is conducted under the conditions set forth in the traffic problems, namely the queue caused by a traffic accident and the impact of a moving bottleneck, described in Section 6.1 and Section 6.2, respectively. The simulation time step is 0.01 seconds. The maximum acceleration is 4 m/s^2 , and the emergency deceleration is 6 m/s^2 in simulations (Ni et al. 2015). Based on simulations, the heat maps of average speed over the time (interval of one second) and the road (interval of 100 m) are calculated, as shown in Figures 10 and 11. Figure 10 shows the simulation results of the

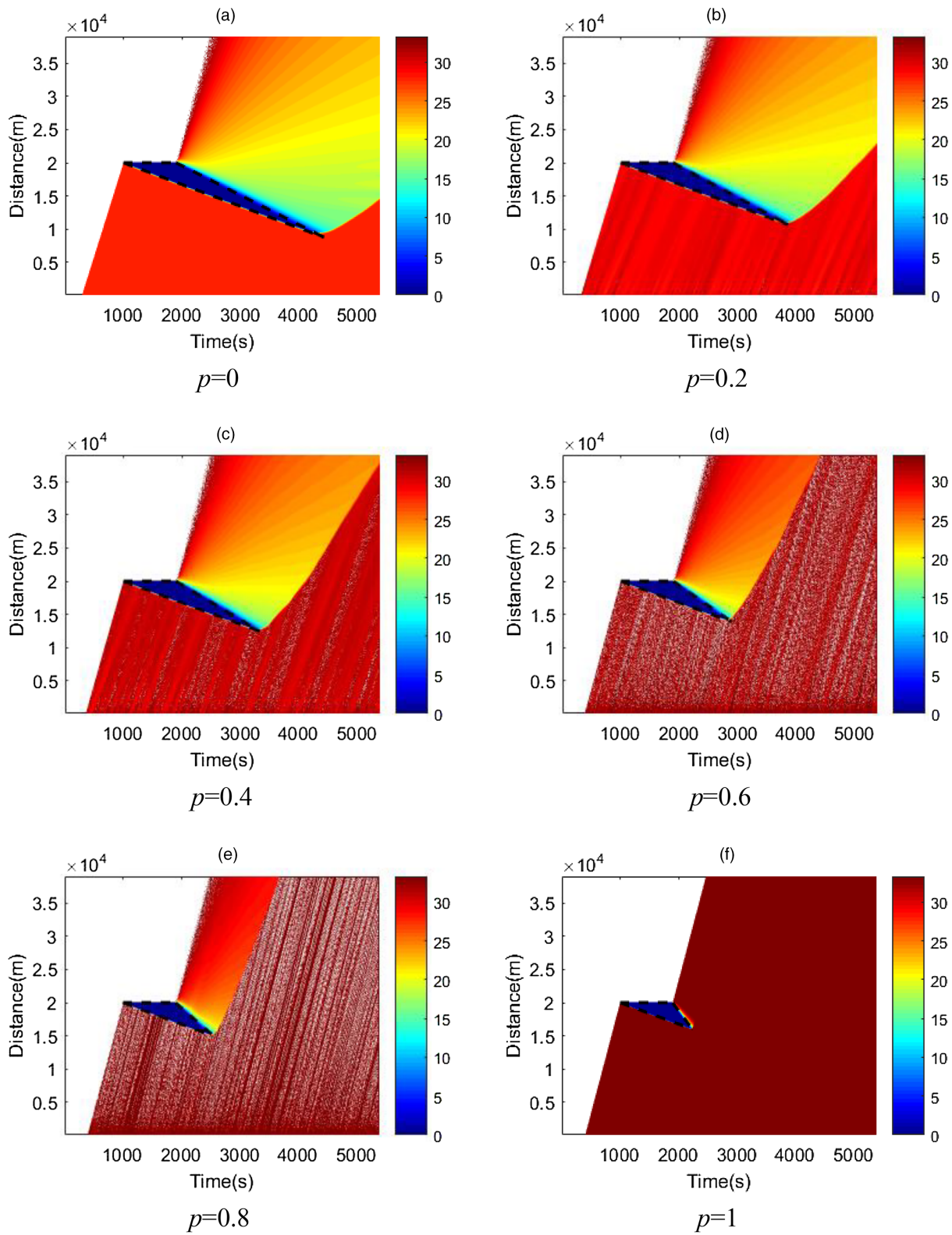
Table 6. Time of Impact for Different CACC Penetration Rates

CACC penetration rate p	Time of impact (hr)	Reduced (%)
$p = 0$	0.3150	—
$p = 0.1$	0.3084	2.10
$p = 0.2$	0.3012	4.38
$p = 0.3$	0.2928	7.05
$p = 0.4$	0.2841	9.81
$p = 0.5$	0.2757	12.48
$p = 0.6$	0.2663	15.46
$p = 0.7$	0.2575	18.25
$p = 0.8$	0.2491	20.92
$p = 0.9$	0.2403	23.71
$p = 1$	0.2251	28.54

traffic accident problem, whereas Figure 11 illustrates the situations of the moving bottleneck problem, under different values of CACC penetration rate p . In Figure 10, the accident occurs at the location of 20 km with the time of 1,000 seconds, whereas the sluggish truck enters the freeway at the location of 10 km with the time of 500 seconds as a moving bottleneck in Figure 11. Because our interest is the impact of the traffic accident or the moving bottleneck on traffic, only simulated vehicle trajectories at locations upstream of the traffic problems are considered to calculate the speed heat maps over time and space. Hence, white color in Figures 10 and 11 means no vehicles running in the time-space area. For the sake of comparison, the analytical results of our mixed LWR model are calculated and illustrated using black dashed lines in Figures 10 and 11.

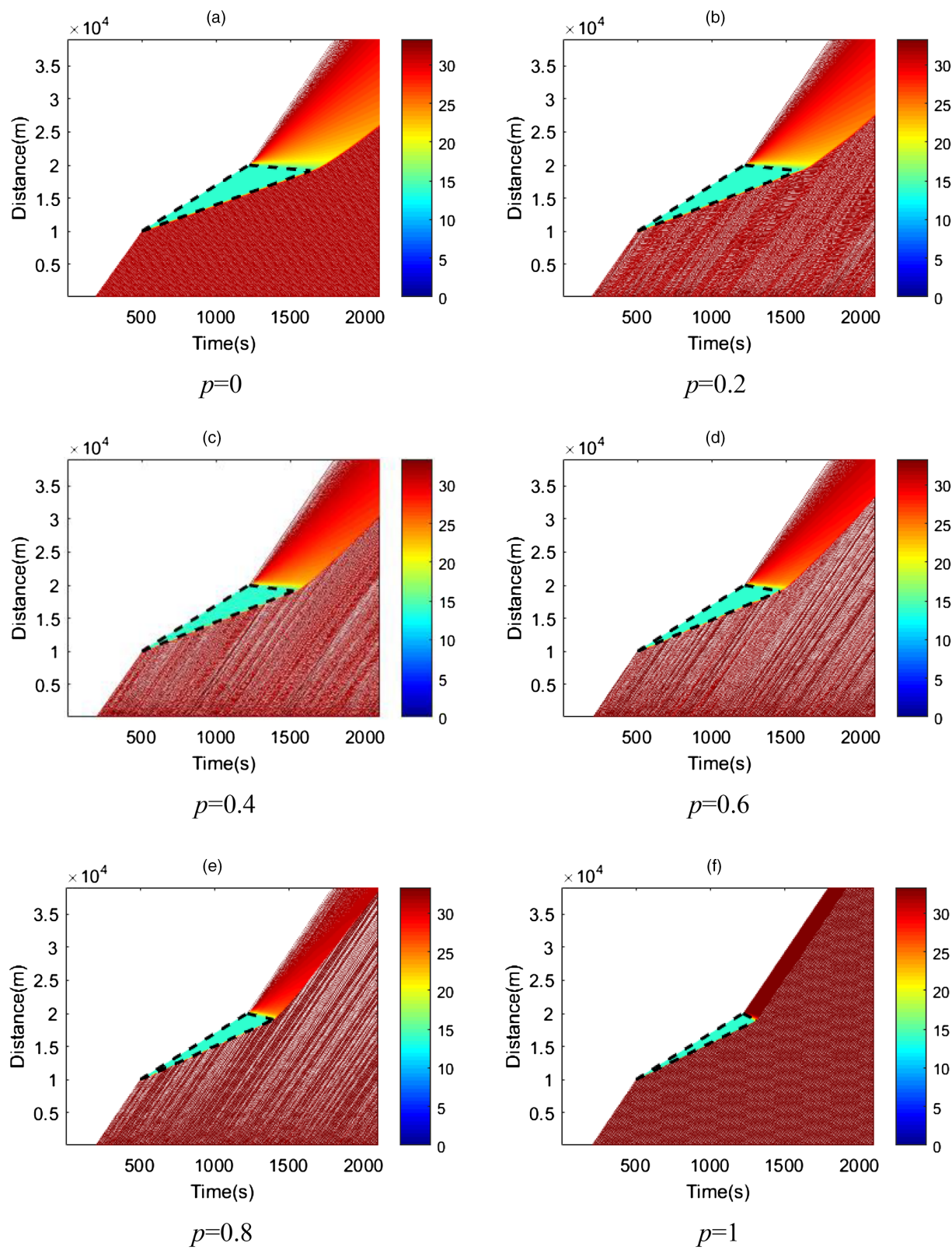
The comparisons are focused on shock waves obtained from both approaches: the shock waves predicted by our LWR model are represented as the dashed lines, whereas the shock waves observed from car following model are naturally revealed as the boundaries of areas with different colors. A good consistency between the car-following model and the new LWR model will be achieved as long as the dashed lines agree with the boundaries of different colored areas. In these examples, our interest is the congested area, which is surrounded by a triangle, where consistency between dashed lines and triangle boundaries is found true. Therefore, the analytical results and the simulation ones are consistent quite well. Random effect of vehicle positions and nonequilibrium car-following dynamics can be seen in simulations. This reveals that our mixed LWR model can match the accuracy from a macroscopic perspective, although it cannot describe the process of nonequilibrium state. More importantly, the analytical results of our mixed LWR model can provide the quantitative comparisons under different CACC penetration rates, as shown in Tables 5 and 6, which is helpful for analyzing the impacts of CACC on traffic problems.

Figure 10. (Color online) Speed Heat Maps of Car-Following Simulations for Traffic Accident Problem



Notes. (a) $p = 0$. (b) $p = 0.2$. (c) $p = 0.4$. (d) $p = 0.6$. (e) $p = 0.8$ (f) $p = 1$.

Figure 11. (Color online) Speed Heat Maps of Car-Following Simulations for Moving Bottleneck Problem



Notes. (a) $p = 0$. (b) $p = 0.2$. (c) $p = 0.4$. (d) $p = 0.6$. (e) $p = 0.8$ (f) $p = 1$.

6.4. Comparison with Multiclass LWR Model

In the existing literature, multiclass LWR models were presented to extend the classical LWR model for mixed traffic flow. Following the general framework, we provide a multiclass LWR model for the mixed flow studied in this paper and evaluate its performance in solving the traffic problems.

In the multiclass LWR model, the conservation of per class is described as

$$\frac{\partial k_u}{\partial t} + \frac{\partial q_u}{\partial x} = 0 \quad \forall u \in \{1, \dots, U\}, \quad (40)$$

where u denotes the class, U is the number of classes, k_u is the density of class u in number of vehicles of class u per length unit, and q_u is the flow of class u in number of vehicles of class u per time unit.

The fundamental relationship of per class can be expressed as follows:

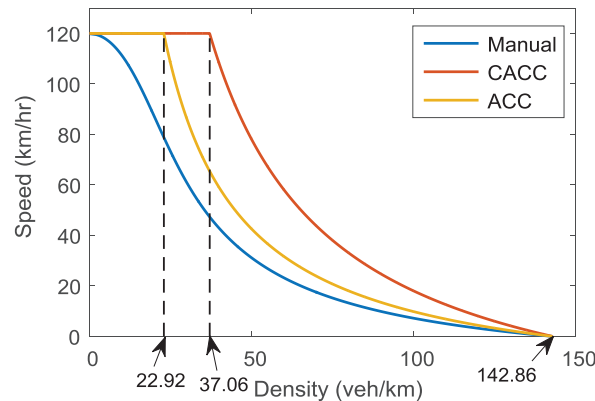
$$v_u = V_u(k_1, \dots, k_U). \quad (41)$$

Equation (39) in most models can be cast in the form $v_u = V_u(k)$, with k the effective density. The effective density k is often the sum of all class-specific densities: $k = \sum_u k_u$. The exact form of the fundamental relationship in Equation (41) is what distinguishes the multiclass models from each other (Loghe and Immers 2008, van Wageningen-Kessels 2016, Qian et al. 2017). In this paper's mixed flow, it is difficult to know the fundamental relationship of future ACC/CACC vehicles. Fortunately, the ACC/CACC car-following models used in our example are validated by PATH's experimental test. Hence, equilibrium relationships derived from the car-following models of the three types of vehicles are used to form $v_u = V_u(k)$ in Equation (41), which can be illustrated in Figure 12.

The time-step finite difference method (FDM) (Wong and Wong 2002) is considered as the numerical solution procedure for the set of partial differential Equation (40). The highway section is evenly divided into cells with the interval of 100 m, and the period of total time is discretized into one-second time intervals. The initial traffic conditions in all cells are considered the traffic demand described in the previous two traffic problems, respectively, in order to evaluate the influence on traffic flow after the traffic accident or the moving bottleneck happens. The results are shown in Figures 13 and 14, in which the speed heat maps over time space are illustrated. Figure 13 shows the performance of multiclass LWR model on describing traffic accident problem, whereas Figure 14 gives the results of the moving bottleneck problem under different CACC penetration rates. For the sake of comparison, the analytical results of our mixed LWR model are also illustrated using black lines in Figures 13 and 14.

Figures 13 and 14 show that the multiclass LWR model can describe the nonlinear dynamics that

Figure 12. (Color online) Relationships Between Speed and Density



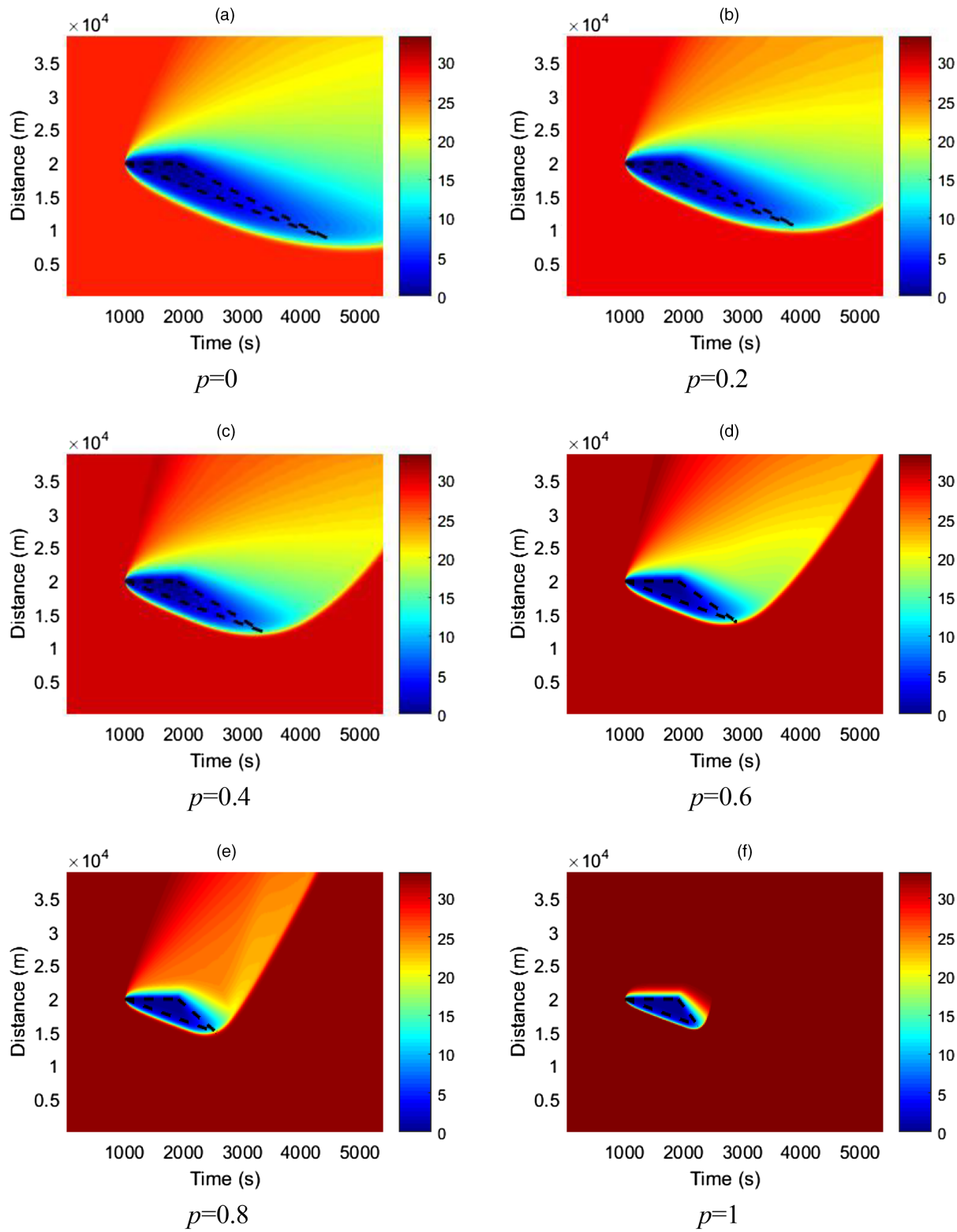
respond to the traffic accident and the moving bottleneck, whereas the analytical results of our mixed LWR model lacks this property. However, our mixed LWR model can provide the analytical shock wave paths for different CACC penetration rates, which has been shown to be consistent with the simulation results of multiclass car-following models in Figures 10 and 11. Moreover, our mixed LWR model is quite simple to solve traffic problems compared with the multiclass LWR model. In addition, we apply the same numerical solution procedure (Wong and Wong 2002) to our mixed LWR model to further examine our model's performance. The results of the traffic accident and the moving bottleneck are shown in Figures 15 and 16, respectively. Based on the comparisons of Figures 13–16, it shows that our mixed LWR model have similar performance with the multiclass LWR model when a numerical solution is conducted. This property further shows the contributions of our LWR model.

6.5. Model Properties and Limitations

The only assumption that we made in our LWR model is the percent of equipped vehicles p , namely the probabilities in Equation (20). The probabilities are of significance from the statistical point of view and should not be interpreted against a specific instant or pattern. Therefore, the probabilities hold no matter whether there are overtaking behaviors, that is, the first in first out (FIFO) assumption is not necessary here.

The presented mixed LWR model is a first-order model and hence is unable to capture some complicated traffic phenomena, such as nonequilibrium features and stop-and-go jams. In order to deal with this, high-order effects may be considered. However, the high-order effects will inevitably complicate the model and make it difficult to solve traffic problems. Therefore, a good balance between high-order effects and the tractability of problem solving should be

Figure 13. (Color online) Speed Heat Maps of Multiclass LWR Model Performance for Traffic Accident Problem

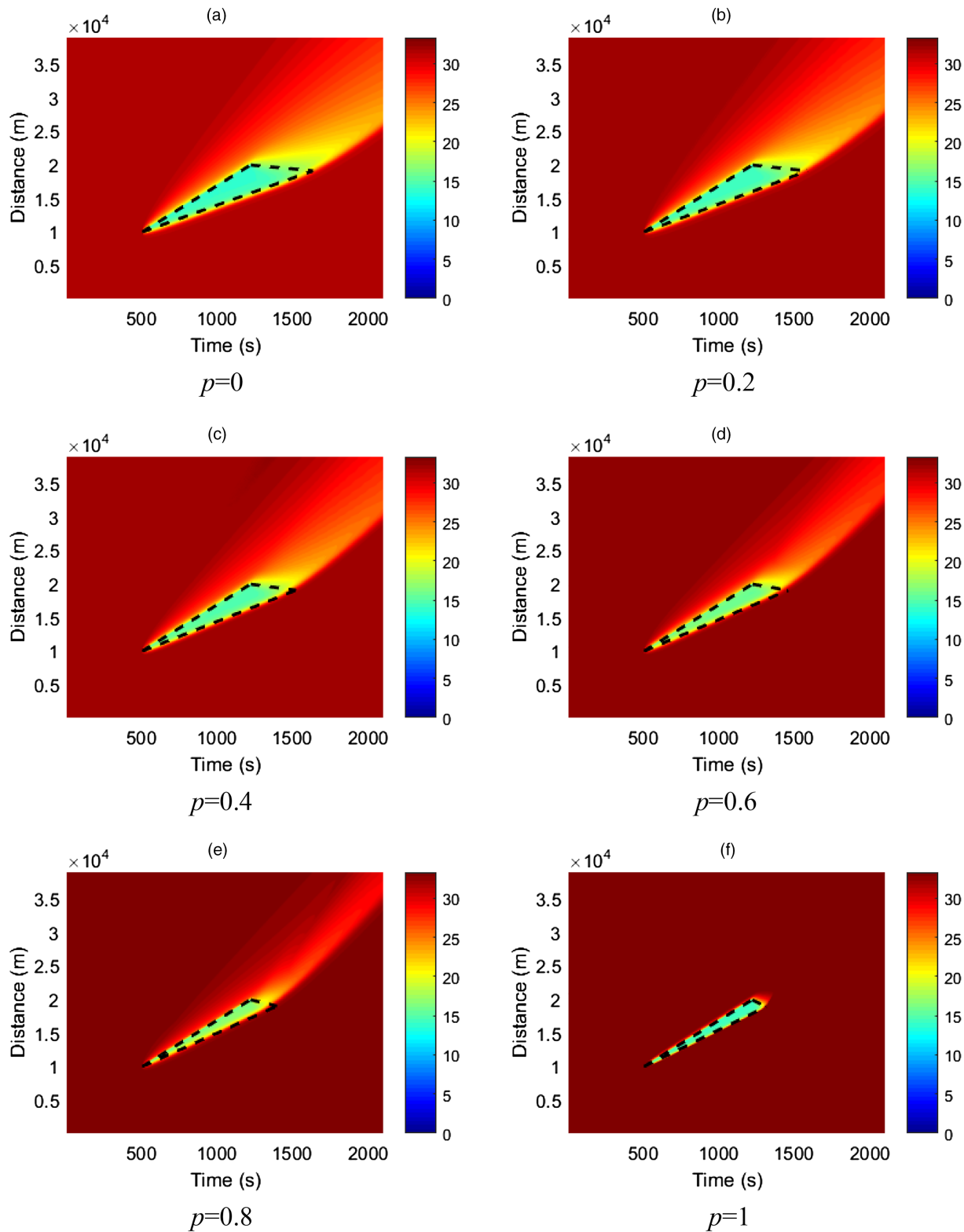


Notes. (a) $p = 0$. (b) $p = 0.2$. (c) $p = 0.4$. (d) $p = 0.6$. (e) $p = 0.8$ (f) $p = 1$.

considered in the future studies. In addition, the proposed mixed LWR model focuses on longitudinal motion of CACC/ACC vehicles in the mixed traffic flow,

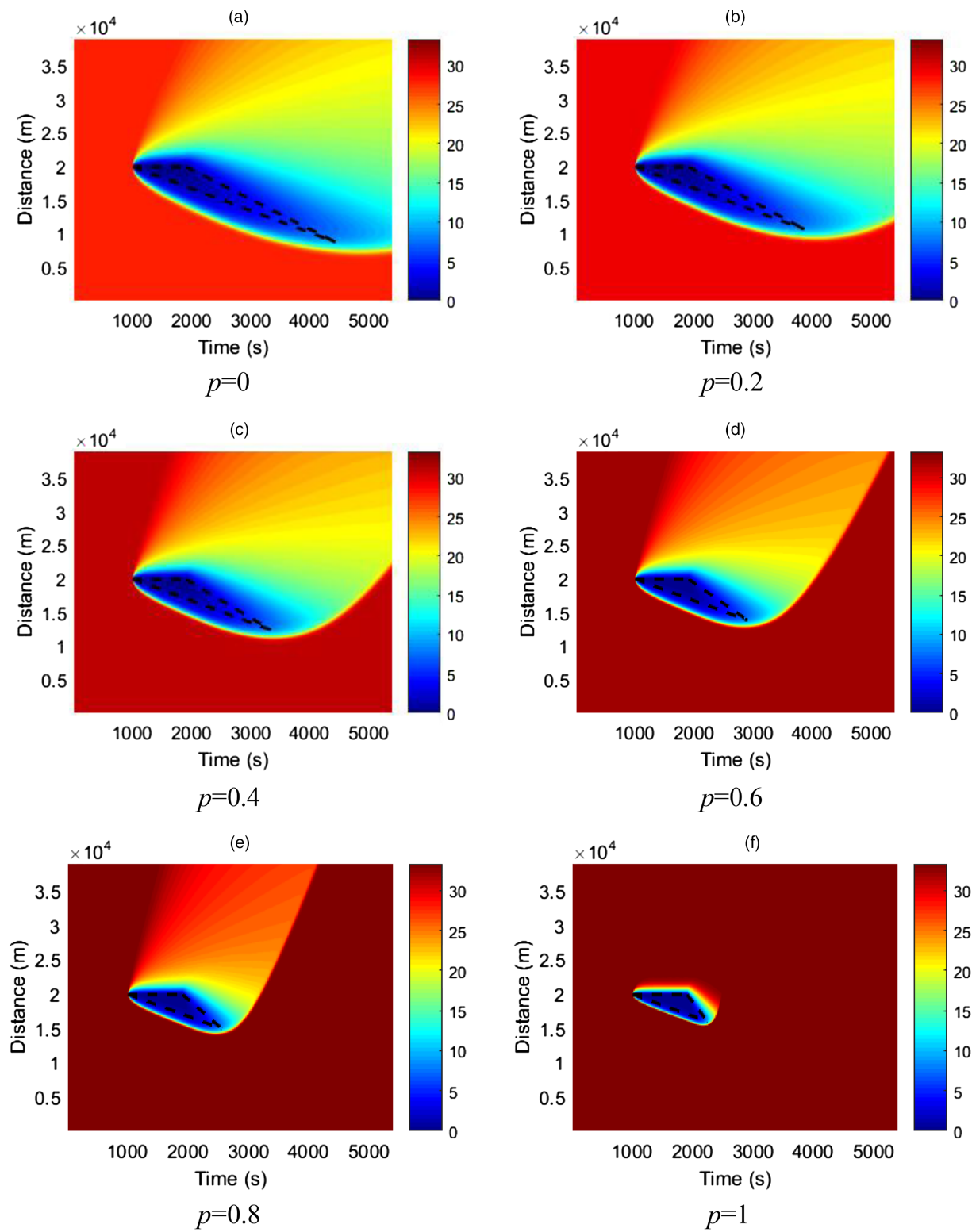
whereas the lateral motion, that is, lane change, is not taken into consideration. The CACC/ACC is initially developed for longitudinal vehicle control, and

Figure 14. (Color online) Speed Heat Maps of Multiclass LWR Model Performance for Moving Bottleneck Problem



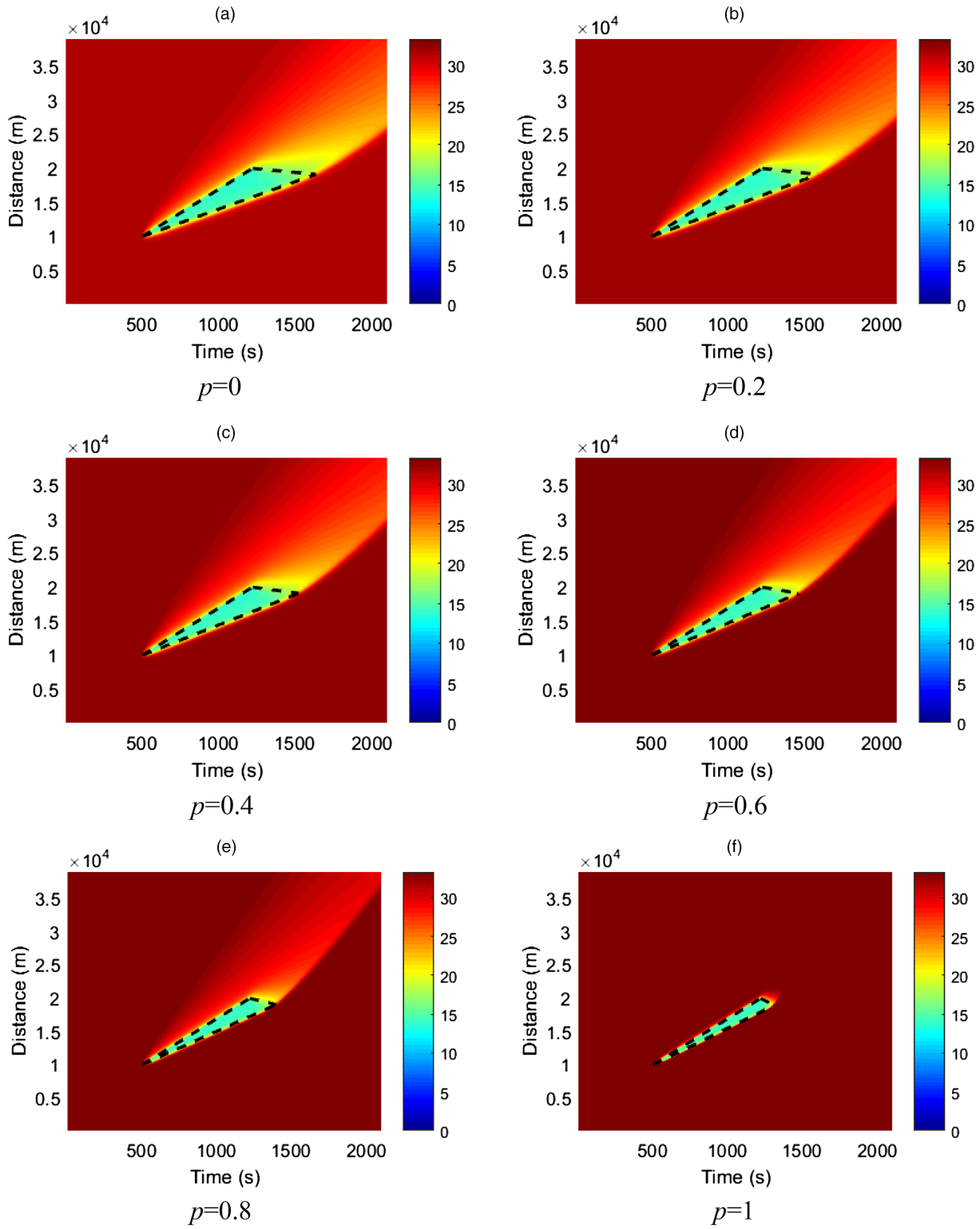
Notes. (a) $p = 0$. (b) $p = 0.2$. (c) $p = 0.4$. (d) $p = 0.6$. (e) $p = 0.8$ (f) $p = 1$.

Figure 15. (Color online) Speed Heat Maps of Numerical Solution of Our Mixed LWR Model for Traffic Accident Problem



Notes. (a) $p = 0$. (b) $p = 0.2$. (c) $p = 0.4$. (d) $p = 0.6$. (e) $p = 0.8$ (f) $p = 1$.

Figure 16. (Color online) Speed Heat Maps of Numerical Solution of Our Mixed LWR Model for Moving Bottleneck Problem



Notes. (a) $p = 0$. (b) $p = 0.2$. (c) $p = 0.4$. (d) $p = 0.6$. (e) $p = 0.8$ (f) $p = 1$.

existing literature generally did not include CACC/ACC system's lane-change behaviors (Milanés and Shladover 2014, Milanés et al. 2014, Shladover et al.

2015, Jia and Ngoduy 2016b, Mahmassani 2016, Talebpour and Mahmassani 2016, Milakis, Van Arem, and Van Wee 2017). The lane-change behaviors of

CACC/ACC involve reoperation, such as clustering and dissolution, which is quite different from that of manual driven vehicles (Shladover et al. 2015). At present, the appropriate lane-change model of CACC/ACC vehicles is still understudied because of its complexity. Therefore, a reasonable lane-change model of CACC/ACC vehicles should be developed first. Then the proposed mixed LWR model can be further studied by taking the lane-change behavior into consideration.

7. Conclusions

In the future, CACC control technologies are expected to improve aspects of traffic flow, such as safety, capacity, and stability. In the random mixed flow, CACC mode will degrade to ACC mode when V2V communications are not available. Although such mixed vehicular flow is likely to be realistic in the near future, properties of LWR model under different CACC vehicle penetration rates have not been adequately studied in existing literature. This paper proposes a generalized framework of analytical investigation of such a mixed LWR model. The kinematic wave speed propagating through a mixed platoon is analytically proven to be the slope of a mixed fundamental diagram under different CACC penetration rates. This means that the mixed fundamental diagram can be used to extend LWR model for such a CACC-manual mixed flow.

Based on three concrete car-following models, the IDM model and CACC/ACC models validated by the PATH program, the derived LWR model can describe the propagation properties of small perturbations quite well. In the case of shock waves, the relative errors between analytical shock wave speed and that of simulation are basically below or only slightly larger than 5%. Although such relative errors are likely to increase to about 30% when shock wave speed comes close to zero, the absolute errors are still very small in those cases. Moreover, the derived mixed LWR model could also solve some LWR problems quite well, such as the queue caused by a traffic accident and the impact of a moving bottleneck. It indicates that CACC vehicles could shorten the queue length by 64.66% and reduce the impact duration of a moving bottleneck by 28.54% under certain traffic flow conditions, when CACC penetration rate increases to one.

Although we used CACC and ACC models validated by the PATH program as examples in this paper, the generalized framework presented in this paper admits other CACC and ACC models when alternative models become available in the future. In addition, the proposed framework of the mixed LWR model can also be used for more advanced CACC systems, for example, the case that CACC vehicles are able to receive information from multiple vehicles beyond the leading vehicle (Ge and Orosz 2014, Fernandes

and Nunes 2015). In that case, the degradation from CACC mode to ACC mode can be more complicated and warrants further study. The investigation on a suitable discrete scheme and then the transformation from such a mixed LWR model to the cell transmission model (Daganzo 1994, 1995; Levin and Boyles 2016a, b) can be the next step. Moreover, the lane-change behavior and the high-order effects can also be considered in further studies.

References

- Benzoni-Gavage S, Colombo RM (2003) An n -populations model for traffic flow. *Eur. J. Appl. Math.* 14(05):587–612.
- Chen D, Srivastava A, Ahn S, Li T (2020) Traffic dynamics under speed disturbance in mixed traffic with automated and non-automated vehicles. *Transportation Res. Part C: Emerging Tech.* 113:293–313.
- Daganzo CF (1994) The cell transmission model: A dynamic representation of highway traffic consistent with the hydrodynamic theory. *Transportation Res. Part B: Methodological* 28(4):269–287.
- Daganzo CF (1995) The cell transmission model, part II: network traffic. *Transportation Res. Part B: Methodological* 29(2):79–93.
- Daganzo CF (1997) A continuum theory of traffic dynamics for freeways with special lanes. *Transportation Res. Part B: Methodological* 31(2):83–102.
- Daganzo CF (2002) A behavioral theory of multi-lane traffic flow. Part I: Long homogeneous freeway sections. *Transportation Res. Part B: Methodological* 36(2):131–158.
- Daganzo CF, Lin WH, Del Castillo JM (1997) A simple physical principle for the simulation of freeways with special lanes and priority vehicles. *Transportation Res. Part B: Methodological* 31(2):103–125.
- Davis LC (2004) Effect of adaptive cruise control systems on traffic flow. *Physics Rev. E* 69(6):066110.
- Delis AI, Nikолос IK, Papageorgiou M (2015) Macroscopic traffic flow modeling with adaptive cruise control: Development and numerical solution. *Comput. Math. Appl.* 70(8):1921–1947.
- Fernandes P, Nunes U (2015) Multiplatooning leaders positioning and cooperative behavior algorithms of communicant automated vehicles for hightraffic capacity. *IEEE Trans. Intelligent Transportation Systems* 16(3):1172–1187.
- Ge JI, Orosz G (2014) Dynamics of connected vehicle systems with delayed acceleration feedback. *Transportation Res. Part C: Emerging Tech.* 46:46–64.
- Ge JI, Avedisov SS, He CR, Qin WB, Sadeghpour M, Gabor O (2018) Experimental validation of connected automated vehicle design among human-driven vehicles. *Transportation Res. Part C: Emerging Tech.* 91:335–352.
- Geiger A, Lauer M, Moosmann F, Ranft B, Rapp H, Stiller C, Ziegler J (2012) Team AnnieWAY's entry to the 2011 Grand Cooperative Driving challenge. *IEEE Trans. Intelligent Transportation Systems* 13(3):1008–1017.
- Gong S, Shen J, Du L (2016) Constrained optimization and distributed computation based car following control of a connected and autonomous vehicle platoon. *Transportation Res. Part B: Methodological* 94:314–334.
- Gong S, Zhou A, Peeta S (2019) Cooperative adaptive cruise control for a platoon of connected and autonomous vehicles considering dynamic information flow topology. *Transportation Res. Record* 2673(10):185–198.
- Guvenc L, Uyan IMC, Kahraman K, Karaahmetoglu R, Altay I, Senturk M, Emirler MT, et al. (2012) Cooperative adaptive cruise control implementation of Team Mekar at the Grand

- Cooperative Driving Challenge. *IEEE Trans. Intelligent Transportation Systems* 13(3):1062–1074.
- Holland EN (1998) A generalised stability criterion for motorway traffic. *Transportation Res. Part B: Methodological* 32(2):141–154.
- Hoogendoorn SP, Bovy PH (2000) Continuum modeling of multi-class traffic flow. *Transportation Res. Part B: Methodological* 34(2):123–146.
- Jerath K, Ray A, Brennan S, Gayah VV (2015) Dynamic prediction of vehicle cluster distribution in mixed traffic: A statistical mechanics-inspired method. *IEEE Trans. Intelligent Transportation Systems* 16(5):2424–2434.
- Jia D, Ngoduy D (2016a) Enhanced cooperative car-following traffic model with the combination of V2V and V2I communication. *Transportation Res. Part B: Methodological* 90:172–191.
- Jia D, Ngoduy D (2016b) Platoon based cooperative driving model with consideration of realistic inter-vehicle communication. *Transportation Res. Part C: Emerging Tech.* 68:245–264.
- Jin WL (2013) A multi-commodity Lighthill-Whitham-Richards model of lane-changing traffic flow. *Procedia Soc. Behav. Sci.* 80:658–677.
- Jin WL (2016) On the equivalence between continuum and car-following models of traffic flow. *Transportation Res. Part B: Methodological* 93:543–559.
- Jin WL, Gan QJ, Lebacque JP (2015) A kinematic wave theory of capacity drop. *Transportation Res. Part B: Methodological* 81:316–329.
- Kerner BS (2016) Failure of classical traffic flow theories: Stochastic highway capacity and automatic driving. *Phys. A* 450:700–747.
- Kesting A, Treiber M (2008) Calibrating car-following models by using trajectory data: Methodological study. *Transportation Res. Record J. Transportation Res. Board* 2088:148–156.
- Kesting A, Treiber M, Helbing D (2010) Enhanced intelligent driver model to access the impact of driving strategies on traffic capacity. *Philos. Trans. Roy. Soc. London A: Math. Physical Engrg. Sci.* 368(1928):4585–4605.
- Kesting A, Treiber M, Schonhof M, Helbing D (2008) Adaptive cruise control design for active congestion avoidance. *Transportation Res. Part C: Emerging Tech.* 16(6):668–683.
- Levin MW, Boyles SD (2016a) A cell transmission model for dynamic lane reversal with autonomous vehicles. *Transportation Res. Part C: Emerging Tech.* 68:126–143.
- Levin MW, Boyles SD (2016b) A multiclass cell transmission model for shared human and autonomous vehicle roads. *Transportation Res. Part C: Emerging Tech.* 62:103–116.
- Li J, Chen QY, Wang H, Ni D (2012) Analysis of LWR model with fundamental diagram subject to uncertainties. *Transportmetrica* 8(6):387–405.
- Lighthill MJ, Whitham GB (1955) On kinematic waves. II. A theory of traffic flow on long crowded roads. *Philos. Trans. Roy. Soc. London A: Math. Physical Engrg. Sci.* 229(1178):317–345.
- Loghée S, Immers LH (2008) Multi-class kinematic wave theory of traffic flow. *Transportation Res. Part B: Methodological* 42(6):523–541.
- Mahmassani HS (2016) 50th anniversary invited article—Autonomous vehicles and connected vehicle systems: Flow and operations considerations. *Transportation Sci.* 50(4):1140–1162.
- Milakis D, Van Arem B, Van Wee B (2017) Policy and society related implications of automated driving: A review of literature and directions for future research. *J. Intelligent Transportation Systems* 21(4):324–348.
- Milanés V, Shladover SE (2014) Modeling cooperative and autonomous adaptive cruise control dynamic responses using experimental data. *Transportation Res. Part C: Emerging Tech.* 48:285–300.
- Milanés V, Shladover SE, Spring J, Nowakowski C, Kawazoe H, Nakamura M (2014) Cooperative adaptive cruise control in real traffic situations. *IEEE Trans. Intelligent Transportation Systems* 15(1):296–305.
- Navas F, Milanés V (2019) Mixing V2V-and non-V2V-equipped vehicles in car following. *Transportation Res. Part C: Emerging Tech.* 108:167–181.
- Ngoduy D (2010) Multiclass first-order modelling of traffic networks using discontinuous flow-density relationships. *Transportmetrica* 6(2):121–141.
- Ngoduy D (2011) Multiclass first-order traffic model using stochastic fundamental diagrams. *Transportmetrica* 7(2):111–125.
- Ngoduy D (2013a) Instability of cooperative adaptive cruise control traffic flow: A macroscopic approach. *Commun. Nonlinear Sci. Numerical Simulations* 18(10):2838–2851.
- Ngoduy D (2013b) Platoon-based macroscopic model for intelligent traffic flow. *Transportmetrica B: Transport Dynamics* 1(2):153–169.
- Ngoduy D, Li T (2021) Hopf bifurcation structure of a generic car-following model with multiple time delays. *Transportmetrica A: Transportation Sci.* 17(4):878–896.
- Ngoduy D, Liu R (2007) Multiclass first-order simulation model to explain non-linear traffic phenomena. *Phys. A* 385(2):667–682.
- Ni D (2015) *Traffic Flow Theory: Characteristics, Experimental Methods, and Numerical Techniques* (Butterworth-Heinemann, Oxford, England).
- Ni D, Leonard JD, Jia C, Wang J (2015) Vehicle longitudinal control and traffic stream modeling. *Transportation Sci.* 50(3):1016–1031.
- Ploeg J, Scheepers BT, van Nunen E, van de Wouw N, Nijmeijer H (2011) Design and experimental evaluation of cooperative adaptive cruise control. *Proc. 2011 14th Internat. IEEE Conf. on Intelligent Transportation Systems* (IEEE, New York), 260–265.
- Ploeg J, Semsar-Kazerooni E, Lijster G, van de Wouw N, Nijmeijer H (2015) Graceful degradation of cooperative adaptive cruise control. *IEEE Trans. Intelligent Transportation Systems* 16(1):488–497.
- Qian ZS, Li J, Li X, Zhang M, Wang H (2017) Modeling heterogeneous traffic flow: A pragmatic approach. *Transportation Res. Part B: Methodological* 99:183–204.
- Rad SR, Farah H, Taale H, van Arem B, Hoogendoorn SP (2020) Design and operation of dedicated lanes for connected and automated vehicles on motorways: A conceptual framework and research agenda. *Transportation Res. Part C: Emerging Tech.* 117:102664.
- Richards PI (1956) Shock waves on the highway. *Oper. Res.* 4(1):42–51.
- Shiomi Y, Taniguchi T, Uno N, Shimamoto H, Nakamura T (2015) Multilane first-order traffic flow model with endogenous representation of lane-flow equilibrium. *Transportation Res. Part C: Emerging Tech.* 59:198–215.
- Shladover SE, Nowakowski C, Lu XY, Ferlis R (2015) Cooperative adaptive cruise control: definitions and operating concepts. *Transportation Res. Record J. Transportation Res. Board* 2489:145–152.
- Talebpour A, Mahmassani HS (2016) Influence of connected and autonomous vehicles on traffic flow stability and throughput. *Transportation Res. Part C: Emerging Tech.* 71:143–163.
- Tang TQ, Wang YP, Yu GZ, Huang HJ (2012) A stochastic LWR model with consideration of the driver's individual property. *Commun. Theoretical Phys. (Beijing)* 58(4):583.
- Treiber M, Helbing D (1999) Macroscopic simulation of widely scattered synchronized traffic states. *J. Phys. Math. General* 32(1):L17–L23.
- Treiber M, Kesting A (2013) *Traffic Flow Dynamics: Data. Models and Simulation* (Springer-Verlag, Berlin).
- Treiber M, Hennecke A, Helbing D (2000) Congested traffic states in empirical observations and microscopic simulations. *Phys. Rev. E* 62(2):1805.
- Van Arem B, Van Driel CJ, Visser R (2006) The impact of cooperative adaptive cruise control on traffic-flow characteristics. *IEEE Trans. Intelligent Transportation Systems* 7(4):429–436.

- Van Lint J, Hoogendoorn S, Schreuder M (2008) Fastlane: New multiclass first-order traffic flow model. *Transportation Res. Record J. Transportation Res. Board* 2088:177–187.
- van Nunen E, Kwakernaat MR, Ploeg J, Netten BD (2012) Cooperative competition for future mobility. *IEEE Trans. Intelligent Transportation Systems* 13(3):1018–1025.
- van Wageningen-Kessels F (2016) Framework to assess multiclass continuum traffic flow models. *Transportation Res. Record J. Transportation Res. Board* 2553:150–160.
- van Wageningen-Kessels F, Van Lint H, Hoogendoorn S, Vuik K (2014) New generic multiclass kinematic wave traffic flow model: Model development and analysis of its properties. *Transportation Res. Record J. Transportation Res. Board* 2422: 50–60.
- Wang H, Qin Y, Wang W, Chen J (2019) Stability of CACC-manual heterogeneous vehicular flow with partial CACC performance degrading. *Transportmetrica B: Transport Dynamics* 7(1):788–813.
- Wang Y, Li X, Tian J, Jiang R (2020) Stability analysis of stochastic linear car-following models. *Transportation Sci.* 54(1):274–297.
- Weinberger M, Winner H, Bubb H (2001) Adaptive cruise control field operational test—The learning phase. *JSAE Rev.* 22(4):487–494.
- Wong GCK, Wong SC (2002) A multi-class traffic flow model—an extension of LWR model with heterogeneous drivers. *Transportation Res. Part A: Policy Practice* 36(9):827–841.
- Xiao L, Wang M, van Arem B (2019) Traffic flow impacts of converting an HOV lane into a dedicated CACC lane on a freeway corridor. *IEEE Intelligent Transportation Systems Mag.* 12(1):60–73.
- Zhang H, Jin W (2002) Kinematic wave traffic flow model for mixed traffic. *Transportation Res. Record: J. Transportation Res. Board* 1802:197–204.
- Zhong ZJ, Lee J (2019) The effectiveness of managed lane strategies for the near-term deployment of cooperative adaptive cruise control. *Transportation Res. Part A: Policy Practice* 129:257–270.
- Zhou Y, Ahn S (2019) Robust local and string stability for a decentralized car following control strategy for connected automated vehicles. *Transportation Res. Part B: Methodological* 125:175–196.
- Zhou J, Zhu F (2020) Modeling the fundamental diagram of mixed human-driven and connected automated vehicles. *Transportation Res. Part C: Emerging Tech.* 115:102614.
- Zhou J, Zhu F (2021) Analytical analysis of the effect of maximum platoon size of connected and automated vehicles. *Transportation Res. Part C: Emerging Tech.* 122:102882.
- Zhong Z, Lee EE, Nejad M, Lee J (2020) Influence of CAV clustering strategies on mixed traffic flow characteristics: An analysis of vehicle trajectory data. *Transportation Res. Part C: Emerging Tech.* 115:102611.